University of Wisconsin Milwaukee

UWM Digital Commons

December 2022

Study of the Various Charactertics of a Helical Vertical Axis Wind Turbine Compared to a Straight Bladed Darrieus Design

Patrick Quinlan
University of Wisconsin-Milwaukee

STUDY OF THE VARIOUS CHARACTERTICS OF A HELICAL VERTICAL AXIS WIND TURBINE COMPARED TO A

STRAIGHT BLADED DARRIEUS DESIGN

by

Patrick Quinlan

A Thesis Submitted In

Partial Fulfillment of the

Requirements for the Degree of

Master of Science

in Engineering

at

The University of Wisconsin-Milwaukee

December 2022

ABSTRACT

STUDY OF THE VARIOUS CHARACTERTICS OF A HELICAL VERTICAL AXIS WIND TURBINE COMPARED TO A STRAIGHT BLADED DARRIEUS DESIGN

by

Patrick Quinlan

The University of Wisconsin – Milwaukee, 2022
Under the Supervision of Professor Ryoichi Amano

As the wind energy market continues to expand, the need for a more diverse range of wind turbine technologies becomes increasingly apparent. Horizontal axis wind turbines (HAWT) have become the standard design for wind turbines over the past few decades and have been the go-to design used in wind farms both on land and off-shore. However, in residential and urban environments other types of turbine designs can help expand the reach of wind energy. Specifically, vertical axis wind turbines (VAWT) have shown potential for new applications of wind turbines in areas that are less suitable for typical HAWTs. The most common VAWT design is the Darrieus turbine, which use a series of straight, vertically oriented blades that rotate around an axis that is perpendicular to the incoming wind. However, this design has shown several disadvantages such as being unable to self-start and creating large amounts of noise. This project seeks to improve these characteristics by adding a helical twist to the blades of a Darrieus wind turbine and evaluating its benefits. With the addition of a helical twist, the gap between each blade begin to decrease as there is now a more fluid transition from one blade to the next as it rotates through the incoming wind. In VAWTs the blades chop through the incoming wind and in front of the center axis, which creates turbulence and causes a fluctuation in the torque produced by the center shaft. Adding a helical twist diminishes this "chopping" motion by allowing for a portion of the blades to nearly always be in front of the center axis.

In order to evaluate the benefits of a helical VAWT, this thesis used a series of live wind tunnel tests and computational fluid dynamic simulations to measure the power output, torque fluctuation, and wake region turbulence of this type of turbine. It compared a helical VAWT with a straight bladed VAWT of the same dimensions. In addition, simulations were used to examine the turbulence in the wake region of the turbines as well as the torque fluctuation produced in the center shaft. The results showed the helical design was found to have an improvement in the power output compared to the straight bladed design and showed improved self-starting capabilities. From the CFD analysis, the helical design did not have any significant improvement in velocity recovery or in the torque fluctuation, and the helical design did only show a slight improvement in the wake region turbulence, which can translate into some noise reduction. The results of this research demonstrate how adding a helical angle to a Darrieus VAWT design improves multiple characteristics compared to its straight bladed counterpart.

TABLE OF CONTENTS

LIST OF FIGURES

LIST OF NOMENCLATURE

Nomenclature:

c   Chord

R   Radius

H   Height

ω Rotation Rate

λ Tip Speed Ratio

P   Power

P_w Power of Incoming Wind

A   Swept Area

σ Solidity

N   Number of Blades

B   Height to Diameter Ratio (H/D)

Abbreviations:

CFD   Computational Fluid Dynamics

HAWT   Horizontal Axis Wind Turbine

VAWT   Vertical Axis Wind Turbine

RANS   Reynolds Averaged Navier Stokes

LES   Large Eddy Simulation

TSR   Tip Speed Ratio

1 Introduction:

In 2021, the Intergovernmental Panel on Climate Change (IPCC) released a report detailing the current state of the Earth's climate and the effect of human influence on the climate. The report stated humans were unequivocally causing climate change and a rise in average global temperatures because of the release of carbon dioxide and other greenhouse gases. It also emphasized an urgency to limit the rise in average global temperature from pre-industrial times to 1.5°C. In order to accomplish this goal, the report recommends an immediate reduction in greenhouse gas emissions. [1] Advocacy for renewable energy has been common for the past 2 two decades, but it has grown significantly since reports such as this one from the IPCC have been released. Renewable sources such as wind, solar, and hydroelectric have expanded greatly in the past decade. In the United States (US) wind energy is leading the way amongst these resources at 43% of renewable energy production, and in total US electricity production, wind holds 8.3%. [2]

This urgency for transition to renewable energy has led to increased demand for wind energy expansion. Wind energy comes in many forms, for example, land-based, offshore, and distributed systems. Diversifying wind turbine technology can drive innovation and expand total capacity as it widens the breadth of applications for wind energy. One such innovation is vertical axis wind turbines (VAWT), where the turbine blades' axis of rotation is perpendicular to the direction of the incoming wind. These types of turbines present some new benefits that make them ideal for applications such as remote residential or farm areas, or for off-grid distributed systems.

VAWTs can come in many forms, but this thesis will examine the Helical VAWT design. Created as an improvement on the Darrieus H-Type VAWT, the helical design aims to reduce torque fluctuations and wake region turbulence by introducing a twist to the blades of the turbines. Two turbine designs

were created for this analysis, a straight H-type and a helical turbine. They were first examined using numerical CFD analysis in Star CCM+. From those simulations a power curve was developed by calculating the power efficiency of each turbine at various rotational rates. The air velocity past the turbine was also measured in order to quantify how much the wind wake needs to return to upstream air velocity. Then to verify the results, next semester 3D printed models of the two turbines will be used in wind tunnel experiments that will utilize a torque meter to directly measure the power produced by the turbines, which will then be used to calculate the power coefficient. Additionally, a hot-wire (HWA) probe will be used to measure the air velocities in the wake region of the turbine.

1.1 Wind Energy:

Wind energy has seen a large increase in the last decade. In 2020, wind capacity grew in the US at a record pace for both land-based and offshore wind turbines. Land-based turbines added 16,836 megawatts (MW) of capacity bringing the total to 121,985 MW. [2] Offshore turbines grew to 35,324 MW total capacity. [3] Globally, wind power capacity has grown to 743 gigawatts (GW), with the U.S. trailing China as the world's second largest wind energy producer. Several countries have reached high levels of wind penetration with Denmark supplying nearly 50% of its total electricity production with wind. [2] Ultimately this rapid growth indicates how much potential and demand there is for wind energy.

Another sector of wind power is distributed wind systems, which are wind turbines that directly serve the end user of the electricity it produces. This can range from residential, commercial, or industrial type users. Turbines in this category typically have a capacity of 100 kW or less. According to the US Department of Energy's report on the distributed wind market, distributed wind systems totaled 1,055 MW of capacity, representing over 87,000 turbines. [4] Figure 1 shows a breakdown of the types of customers that use these small turbines.

US Distributed Wind System Capacity

Residential and Agricultural, 2.0%

Government, 1.5%

Commercial, 1.5%

Industrial, 37.0%

Utility, 58.0%
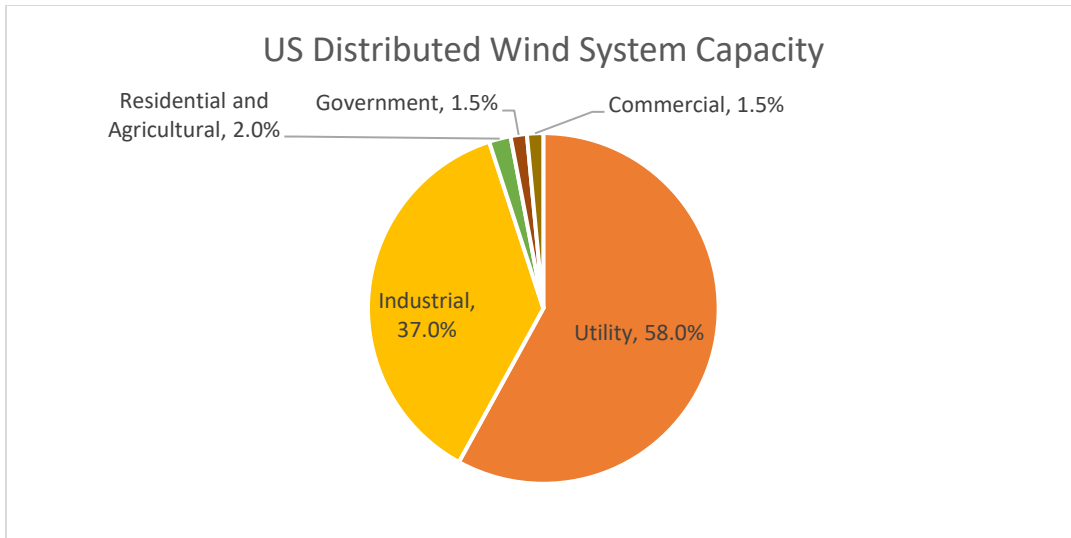
FIGURE 1: BREAKDOWN OF DISTRIBUTED WIND SYSTEM CUSTOMERS [4]

The Department of Energy also estimates that distributed wind systems are technically feasible for approximately 49.5 million residential, commercial, or industrial sites, which represents 44% of all US buildings. [4] This data demonstrates the potential for distributed wind systems and how it can be a viable option for wind energy projects. In addition, distributed wind systems have the benefit of not requiring large infrastructure and power transmission since their turbines directly serve its end users. According to a study by the Ernest Orlando Lawrence Berkeley National Laboratory, the median cost of power transmission for all project scenarios analyzed was $300/kW, or 15% of the total project building cost. [5] Thus, under certain conditions, distributed wind systems can be incredibly beneficial for some buildings, such as remote homes and farms, residential communities and neighborhoods, and areas affected by natural disasters.

Wind turbines typically follow two design categories: horizontal axis wind turbines (HAWT) and vertical axis wind turbines (VAWT). HAWTs are the most common design where the axis of rotation of the turbine blades are parallel to the direction of the wind, while VAWTs' blades are normal to the direction of the wind. HAWTs have the advantage of being more efficient and more commercially exploited for large scale power production both land-based and offshore. [6]
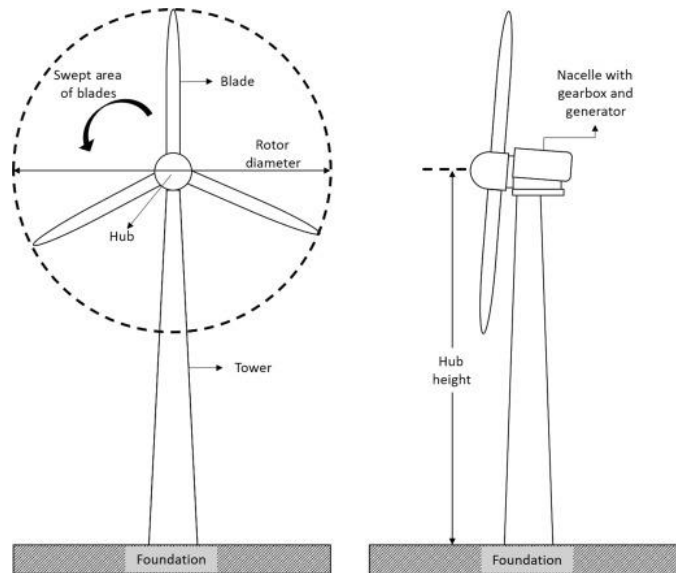
FIGURE 2: DIAGRAM OF A HORIZONTAL AXIS WIND TURBINE

However, these turbines have some disadvantages that make them impractical for certain wind project applications. For example, their size contributes to difficulties in transport, installation, and maintenance. Additionally, they require a yaw system to turn the blades in the direction of the wind, which adds costs and points of failure. The primary benefits of VAWTs are they are omni-directional, and therefore do not require a yaw system, they have lower manufacturing costs, produce less noise, and their generator can be placed on ground level, which adds an element of safety for maintenance workers. [6] Given these characteristics, VAWTs are ideal candidates for distributed wind systems.

Many designs and configurations have been made for VAWTs, but this study will focus on two versions of Darrieus wind turbines, which are lift-based that use airfoil blades, similar to airplanes, and HAWTs. These designs were invented and patented by French aeronautical engineer Georges Jean Marie Darrieus. [7] The following figure shows the various designs he created.
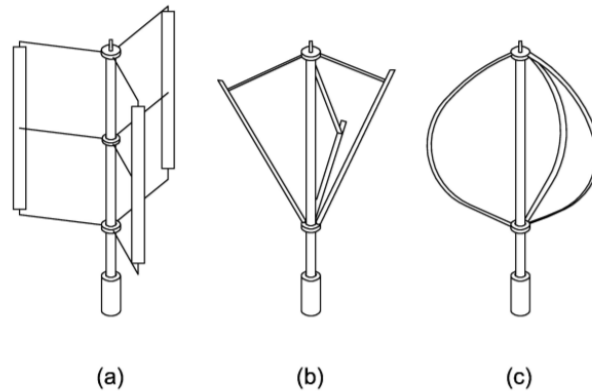
FIGURE 3: DARRIEUS VAWT DESIGNS: A) H-TYPE B) V-TYPE C) TROPOSKEIN TYPE [8]

The H-Type design was then modified by Alexander Gorlov, who created a helical blade design where the turbines would twist along the vertical axis. While originally designed for hydro-turbine applications, Gorlov developed this turbine to smoothen torque fluctuation, and he noted in his research the potential in wind turbine application. [9] The goal of this design is to more evenly distribute the forces of the blades around the center axis. This can lead to several benefits which will be examined in this thesis report. Firstly, it can reduce the fluctuation in torque of the turbine, which can help decrease fatigue in the turbine assembly and reduce the need for maintenance. Secondly, it can reduce the turbulence of the turbine wake, which can lead to less aerodynamic noise. Less turbulence can also allow for turbines to be stationed in closer proximity, which is beneficial for wind farm applications.

Studies on the helical turbine have found some drawbacks in the design as well. Baker [10], for example, found the forward leaning twist of the helical blades introduces a spanwise flow component in 3D flow, which reduces the lift coefficient of the blade. There are also claims that the cost of manufacturing a helical blade would be higher since instead of employing a well-established aluminum extrusion method for manufacturing the blades, the process is limited to molding. [11] However, this thesis will examine if the benefits of a helical design outweigh the drawbacks.

5

2 Literature Review:

This thesis compares the design characteristics of the Darrieus H-type and the helical VAWTs. These designs were evaluated on their efficiencies, fluctuations in torque, and wind wake recovery. How these designs were evaluated is covered in the next section. The genesis of this research comes from a lack of studies that directly compare these two designs. Each design has been studied individually, discovering all their qualities and failings, but there are few that directly compare them. Much of the research of VAWTs focus on the efficiencies of the turbines when there are many other factors to consider for these types of designs, such as fatigue life, turbulence in the wind wake, and noise.

Darrieus H-Type VAWTs have been extensively studied and show a typical power coefficient of 0.30 to 0.40. [6] The main issues with VAWTs are their starting torque, mechanical vibrations, and vortex generation in their near-wake region. Many different designs have been proposed to mitigate these issues. The helical VAWT aims to improve the mechanical vibration and vortex generation by introducing a helical twist to a Darrieus H-Type. Initial studies on this type of design by Alexander Gorlov were conducted for hydro turbines. [9] Shiono studied the helical design under hydro conditions and found it had a better starting torque than a straight H-type design and that the optimal twist angle for the helical design was 43.7°. [12] One issue with these studies, however, is they are performed under hydro applications, and it cannot be assumed these results will directly translate to wind turbine conditions.

In the study, *Effect of Helix Angle on the Performance of Helical Vertical Axis Wind Turbine*, Divakaran used CFD simulations to examine the characteristics of four different VAWTs with varying helical angles. They also studied the wake region turbulence of the turbines.
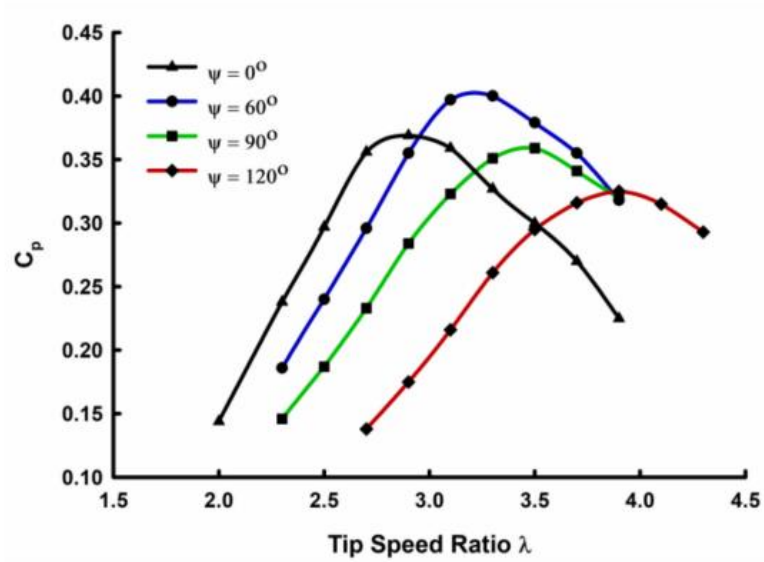
FIGURE 4: PLOT OF POWER COEFFICIENT OF DIFFERENT HELICAL TURBINES [13]

Figure 4 shows the plot of the power coefficients of each turbine, and the 60° turbine performed the best out of all the designs, even compared to a turbine without any helical twist. [13] The study also used the moment coefficient to evaluate the torque fluctuation.
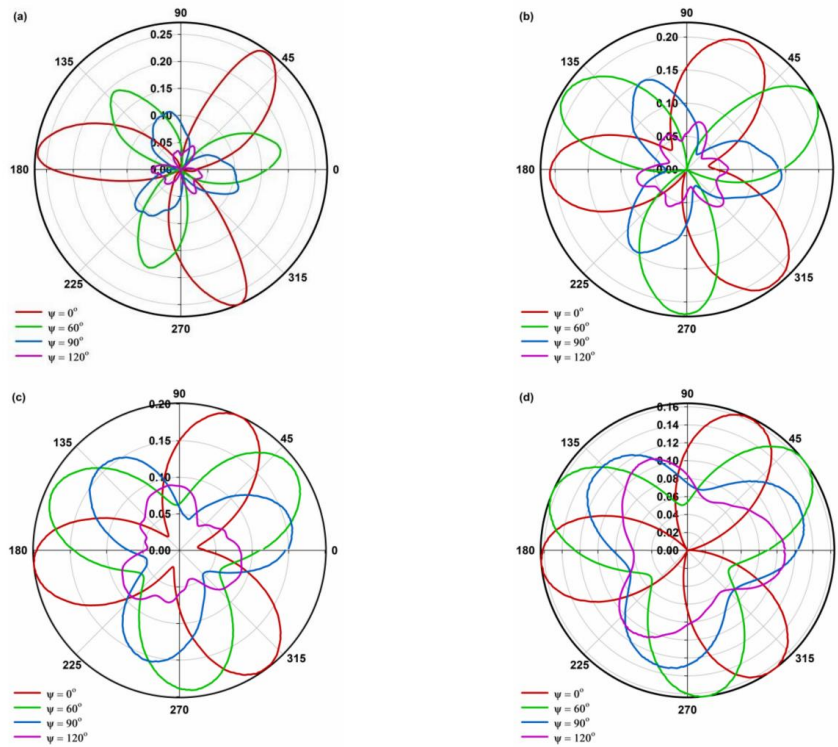
FIGURE 5: POLAR PLOT OF MOMENT COEFFICIENT COMPARING DIFFERENT HELICAL ANGLES AND A STRAIGHT BLADE AT (A) TSR = 2.3 (B) TSR = 2.5 (C) TSR = 3.1 (D) TSR = 3.5 [13]

Figure 5 are the polar plots from Divakaran that plot the moment coefficient of each design at multiple TSRs. They illustrate how adding a helical angle lowers the moment coefficient. While this is a useful result, the torque fluctuation can be better quantified using the equation:

$$Fluctuation = \frac{|T - T_{avg}|}{T_{avg}}$$

This equation was used by Cheng to calculate the torque fluctuation of a helical bladed VAWT. Cheng conducted an experiment in both 2D LES and 3D U-RANS simulations and a live wind tunnel experiment for validation of a 4-bladed helical VAWT with a twist angle of 70°. Tests were conducted at multiple TSRs and an inlet velocity of 9 m/s. The results showed a maximum power coefficient at a TSR of 1.8, and the torque of the turbine fluctuated more at lower TSRs. [14] Ultimately, this study emphasizes the importance of selecting an optimal TSR for helical VAWTs. One gap in this paper's research is a lack of

direct comparison to a straight-bladed VAWT. Such a comparison would have given better context for the benefits of a helical blade on vortex generation and blade-wake interaction. Additionally, 4-bladed Darrieus turbines have been shown to have marginally higher power outputs than 3-bladed turbines, which does not justify the added costs of manufacturing a fourth blade. [15] Therefore, finding the optimal TSR for a 3-bladed helical turbine would have been more valuable. This study, however, does provide a good framework for numerical analyses of VAWTs, and this thesis models its simulations similar to Cheng's parameters.

In "Numerical Study of the Aerodynamic Performance of a 500W Darrieus-Type Vertical-Axis Wind Turbine", Lee evaluated the performance of a 3-bladed vertical H-type 500W wind turbine in both numerical analyses and in experimental methods, and tests were also run for helical designs at varying twist angles. Lee found the straight H-type had power coefficients between 0.30 - 0.38, depending on the blades' solidity parameters, and the maximum power output occurred at a TSR of 1.6. [16] Lee also found the straight H-type design performed better than the helical designs with respect to power coefficient, with the helical designs having a maximum efficiency of 0.31 at a TSR of 2. [16] However, this study had a few gaps in its experiments. Firstly, this study only compared power coefficients when comparing designs, which can be a limited view on these turbines' qualities. Second, experimental tests were only conducted on the straight H-type turbine and none were conducted on a helical design. These tests are meant to verify the results of the numerical analyses and omitting them leaves the research incomplete. Additionally, the numerical analyses of the helical designs only covered twist angles up to 30 degrees when other studies have shown the optimal twist angle for a helical design is 60°. [13]

The studies reviewed in the section examine many different aspects of the helical VAWTs, but each seem to have left some incompleteness in their evaluation. This thesis seeks to fill that gap by directly comparing the straight H-type design and helical design across multiple characteristics, including power efficiency, wake recovery, and torque fluctuation.

3 Research Summary:

This study of the helical VAWT design uses a combination of live wind tunnel experiments and 3D CFD simulations to evaluate several characteristics. The goal of this research is to quantify the benefits of adding a helical angle to a typical Darrieus straight bladed VAWT design. An initial analysis was first conducted to verify past research results and determine the optimal helical angle for the design. Models of three helical designs with angles of 30°, 60°, and 90° as well as a straight bladed model were first created in a CAD software and then imported into Star CCM+. Using a Large Eddy Simulation (LES) analysis, the turbines were simulated under inlet air velocities of 5, 7, 9, 10, and 12 m/s and set to rotate at the specified rotation rated from a given TSR of 1. The simulation ran for one second of rotation. This allowed adequate time for the solution to develop and stabilize. During the simulation, the torque was measured along the shaft of the turbine. From the extracted data, the average torque is calculated and used with the rotation rate to find the output power. The design with highest power output is then used for the wind tunnel experiments to be compared with the straight-bladed turbine design. Additionally, the fluctuation in torque is quantified by finding the difference in instantaneous torque to the average torque over the same revolution span. The torque fluctuation acts as a good indicator for fatigue in the turbine and adds another point of quality comparison between the designs.

While most of the results were extracted from the CFD simulations, the experiments in the wind tunnel had several goals. First, the rotation rates of each turbine provide a necessary parameter for the numerical simulations used to recreate the results of the wind tunnel experiments. Second, the wind tunnel was used to test the self-starting capabilities of the straight bladed and helical bladed designs. Models of the turbine designs were 3D printed using a AnyCubic Chiron 3D printer. The models were 1:1 scale to ensure the most comparable results. Spokes were added to connect the blades to the center

shaft, but these features were omitted from the initial simulation models. Figure 6 below shows a

sample image of the 3D print models.

FIGURE 6: MODEL OF THE STRAIGHT H-TYPE TURBINE FOR WIND TUNNEL EXPERIMENTS

The numerical simulations were conducted in Star CCM+. They model two fluid domains, a large

domain to represent the surrounding flowing air and a rotating domain that represents the fluid

immediately surrounding the turbine. The outer wind tunnel domain has a specified inlet which sets the

velocity of the incoming wind and a pressure outlet. The domain was made large enough, so the walls

do not influence the flow around the turbine. The inner rotating domain that houses the turbine was set

to the corresponding rotation rate from the wind tunnel experiments. This was done for the helical

design and the straight bladed design. The first item the simulations examined was the power output of

the turbines. This was done by measuring the torque on the blades and center axis of the turbine and

multiplying this value with the rotation rate. The torque measurements were also used to evaluate the

torque fluctuation of each turbine design. The forces experienced by each blade were also measured

individually. This was used to give insight into the self-starting capabilities of each design. The

simulations were then used to model the behavior of the wake region airflow in order to evaluate the velocity recovery and level of turbulence. The goal of the helical design is to dampen the turbulence in the wake region which can improve characteristics such as noise.

4   Design Parameters:

The first parameter decided for the turbine design was the airfoil profile. Since the scope of this research focused on evaluating a helical design, an airfoil was chosen that is common among similar designs and near optimal in terms of efficiency. Considering these criteria, the NACA0018 profile was chosen, which is a symmetrical airfoil widely used in VAWT design. This profile was also used in many of the studies reviewed in the Literature Review section. This profile has also been found to be one of the most optimal for VAWTs. In a study by Modi, various airfoils were simulated in 2D for a three-bladed VAWT and found NACA0018 and NACA0024 had the highest power coefficient among the five that were tested. [17] The study also found asymmetric profiles have efficiencies near the symmetric profiles as well, which presents some potential when considering cut-in speeds for VAWTs. However, this thesis will not examine asymmetric airfoils.

The primary dimensions of the VAWTs used in this research are the height, diameter, and chord length. In order to maintain a 1:1 scale between the simulations and the wind tunnel experiments, the height and diameter are limited by the dimensions of the wind tunnel test section. The height of the turbine is set to 250 mm. This dimension was chosen for two reasons. First, the turbine needs to be small enough to have an adequate distance from the walls of the test section to avoid influence on performance. Secondly, the experimental turbine was fabricated with a 3D printer; thus, it is limited to the dimensions of the printer. From the height, the diameter is determined using the chosen height-to-diameter ratio (H/D or β), 0.85. This value was chosen based on the research from Bianchini where the

optimal H/D of a H-Darrieus VAWT with profile NACA0018 was found to be 0.85. [18] The number of

blades was set to three. According to Castelli, three is the optimal number of blades for a straight

Darrieus H-type wind turbine as it showed the highest power coefficient. [15] Adding a fourth blade

does increase power output, but only marginally. Factoring in manufacturing cost, a fourth blade proves

to have no net benefit.

The chord length of the blades is calculated using the optimal solidity of the turbine. Solidity is

defined as the ratio of blade surface area to the frontal, swept area that the rotor passes through. This

can be seen in the following equation:

$$\sigma = \frac{Nc}{2\pi R}$$

(1)

The solidity was set to 0.3, as the optimal range for solidity to extract maximum energy lies between

0.25 and 0.4. [6] From Eqn. 1 the chord length, c, is solved for, giving the following equation:

$$c = \frac{\sigma\pi D}{N}$$

(2)

In a similar fashion to the chord length, the rotation rate of the VAWT was determined from the

optimized value for the TSR (λ).

$$\lambda = \frac{\omega R}{U_\infty}$$

(3)

From this equation, the rotation rate (ω) is solved for in the following equation:

$$\omega = \frac{\lambda U_\infty}{R}$$

(4)

The range of inlet air velocity was set to 5, 7, 9, 10, and 12 m/s for this study. The TSR was examined at

multiple values to develop a power curve using the final results, which compares the inlet velocity to the

power coefficient. In each simulation, the turbine was set to rotate at the specified rotation rate for one

second. From there the average torque was calculated. The average torque was used because the

instantaneous torque value oscillates as the turbine rotates around the center shaft. This value was then

used to calculate the average power by multiplying it by the rotation rate.

$$P = T_{avg} * \omega$$

(5)

The power coefficient could then be calculated by normalizing this value to the maximum available

power in the wind, which found using the following equation.

$$P_{wind} = \frac{1}{2} \rho_{air} A v^3$$

(6)

A is the swept area of the turbine, which for a VAWT is calculated as follows:

$$A = H * D$$

(7)

The torque fluctuation was also evaluated for each turbine. This determined by comparing the

instantaneous torque to the average torque over the same 3 revolution span.

$$Fluctuation = \frac{|T - T_{avg}|}{T_{avg}}$$

(8)

5 Computational Fluid Dynamics:

5.1 Preliminary CFD Analysis for Optimal Helical Twist Angle:

The numerical analysis in this study was conducted using Star CCM+. Models for the wind turbine were first made in Inventor Pro and exported as STEP files. As described in the design parameters, each turbine was constructed with 3 blades at a height of 250 mm. A center axis pole with a diameter of 10 mm was added to represent the center shaft of the turbine and account for its aerodynamic effects. As covered in the Literature Review, a study from Divakaran found the optimal angle of twist for a helical VAWT design was 60°. [13] To verify this study, a set of simulations were run for helical designs at three different angles of twist, 30°, 60°, and 90°.

5.1.1 Computational Domain Construction:

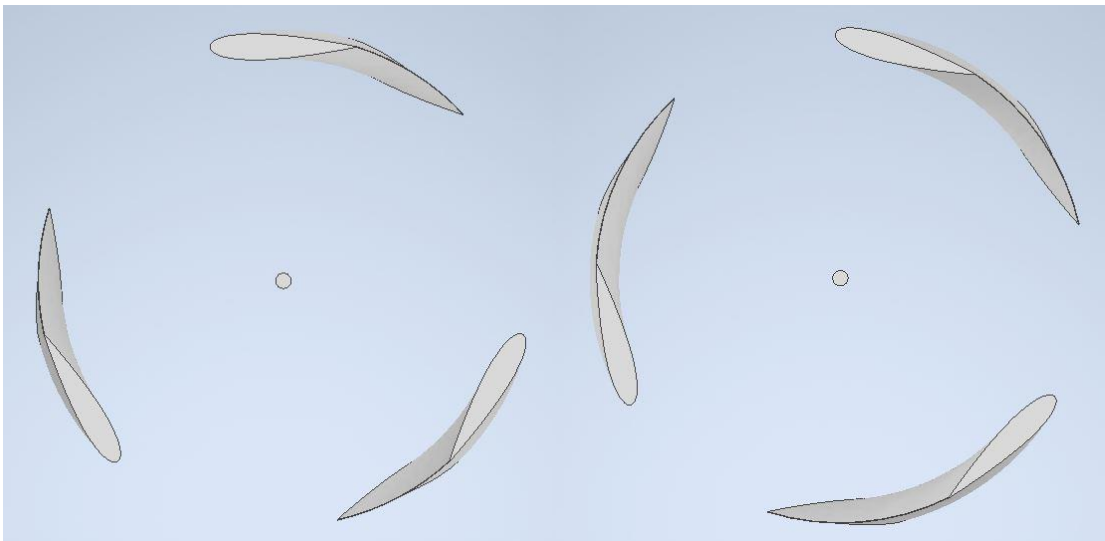Models of each angle were created and imported into Star CCM+.

FIGURE 7: 30 DEGREE DESIGN (LEFT) AND 60 DEGREE DESIGN (LEFT)

15

The spokes connecting the blades to the center shaft were excluded to simplify the simulations at this early stage. The computational domain was divided into two regions: the inner rotating domain and the outer wind tunnel domain. The radius of the inner rotating domain was set to 1.3R and the height was set such that there was 100 mm of space above and below the turbine. This region encompasses the mesh closest to the turbine and therefore was set to a much higher mesh density then the base mesh size. The outer wind tunnel domain acted as the surrounding fluid flowing across the turbine. One face of this region was set as the air velocity inlet, and the face on the opposite end was set as the pressure outlet. The left and right sides of the block were set as symmetry planes, so they do not create a boundary layer and influence the airflow over the turbine. The inlet was set to a distance 15R away from the center of the wind turbine, while the outlet was set to a distance 40R away. The total width of the domain was set to 20R. These dimensions allow for adequate distance for the air flow to pass the turbine and return to uniform flow without any significant interference from the walls of the domain. Figure 9 details the domain dimensions.
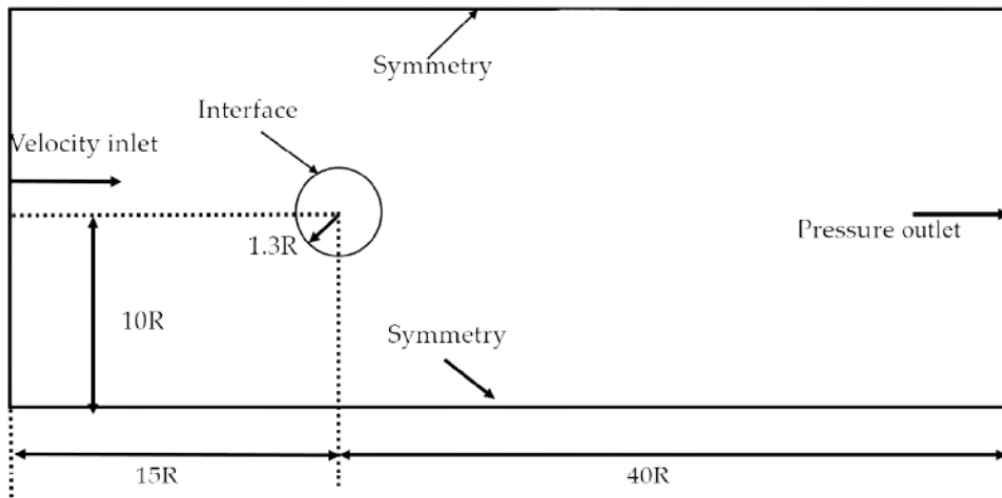
FIGURE 9: FLUID MESH DOMAIN DIMENSIONS

Each model was simulated at wind speeds of 5, 7, 9, 10, and 12 m/s. To find the corresponding

rotation rate, a TSR of 1 was assumed since it is a typical TSR for VAWTs. The inner rotating domain was

set to rotate along the Y axis while the wind tunnel domain remained stationary. The torque output was

measured on the blade surfaces in the simulations. From those results, the average power was

calculated and then the power coefficient, as detailed in *Design Parameters*.

5.1.2 Mesh Generation:

The accuracy of CFD simulation heavily depends on the density of its mesh, especially in the

regions and surfaces it is examining. In this research the area most important is the region around the

turbine blades and the wake region past the turbine. Below is a top section view of the 90° Helical
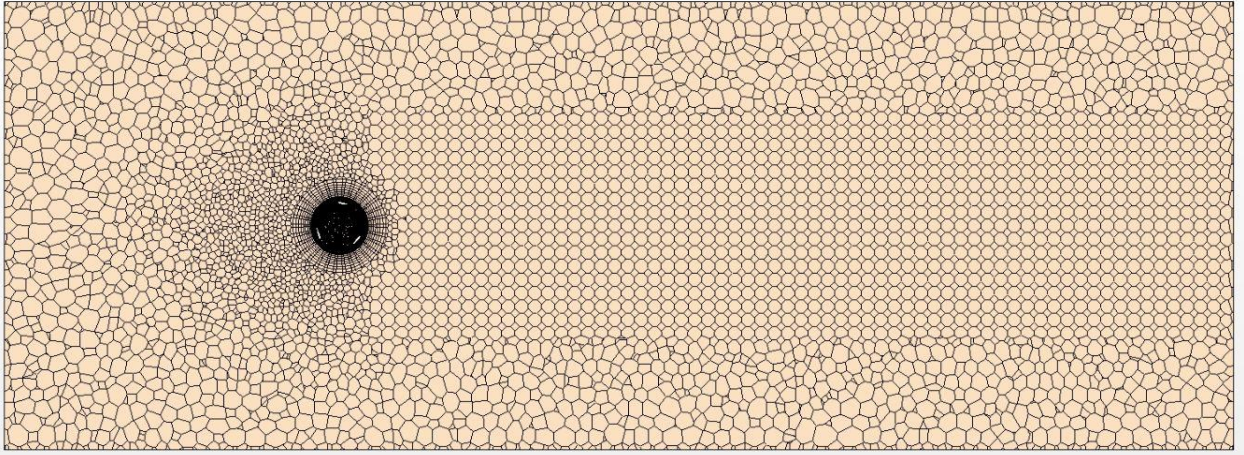
turbine.

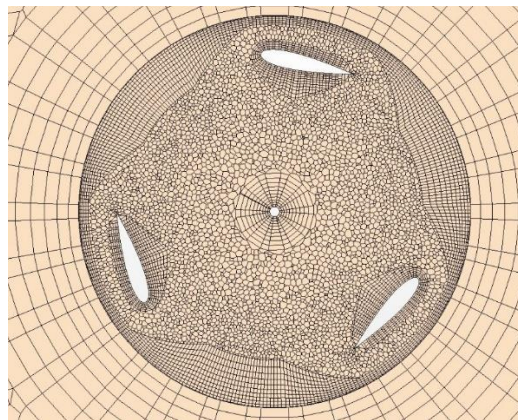**FIGURE 10: TOP SECTION VIEW OF THE 90 DEGREE HELICAL TURBINE MESH**

FIGURE 11: ZOOMED IN VIEW OF 90 DEGREE HELICAL MESH NEAR TURBINE BLADES

In Figure 10 there are two areas where the mesh is more refined: in the inner region that houses the

turbine and the wake region past the turbine. A fine mesh around the surface of the turbine allows for a

more accurate analysis of the air flow and vortices around the walls of the blades. The model also has 10

prism layers set to each solid boundary around the turbine and at the interface between each region.

Similarly, a finer mesh in the wake region allows for a more accurate look at the vortices generated in

the air flow past the turbine. However, analyzing the wake region is less significant for this initial study

18

since it only examines the power output from the turbine. A polyhedral mesh was used for mesh was

chosen for this research since it provides the most accurate while having a shorter run time compared to

a tetrahedral or a hexahedral mesh. Table 1 details the mesh statistics of each model used in this study.

Mesh Statistics	
Helical Twist	**Mesh Cell Count**
30 Degree	1,355,576
60 Degree	2,348,520
90 Degree	1,435,343

TABLE 1: MESH STATISTICS FOR HELICAL TWIST ANALYSIS MODELS

5.1.3 Physics Model Selection:

Another important parameter for the CFD simulations were the physics models chosen for the

mesh. Two different types of physics models were used in this research. First, a Large Eddy Simulation

(LES) was chosen because it can successfully deal with the various eddies in the air flow around the

rotating turbine blades, for both large and small scale. Since this study uses incompressible flow, a

segregated flow model was used with the SIMPLE-type algorithm for pressure-velocity coupling. LES

does require more computational effort, but it has been shown to more accurate in modeling the wake

region of wind turbines. [19] The other type of model used was a Reynolds Averaged Navier Stokes

(RANS) model. In these models, the Navier-Stokes equations for the instantaneous velocity and pressure

fields are decomposed into a mean value and a fluctuating component. This produces an extra term

known as the Reynolds stress tensor which is modeled as turbulent viscosity.

The physics models also have the airflow set to a turbulent flow which sets the Reynolds

number to a value greater than 4000. VAWT are typically placed in areas with very turbulent air.

Considering their characteristics, such as being omnidirectional, they are ideal for environments where

air is highly volatile and turbulent. This type of physics modeling also allows for more accurate

renderings of the turbulent air generated after the turbine.

5.1.4 Preliminary Analysis Results:

Compiling the results from every simulation, the final power coefficient for each model is
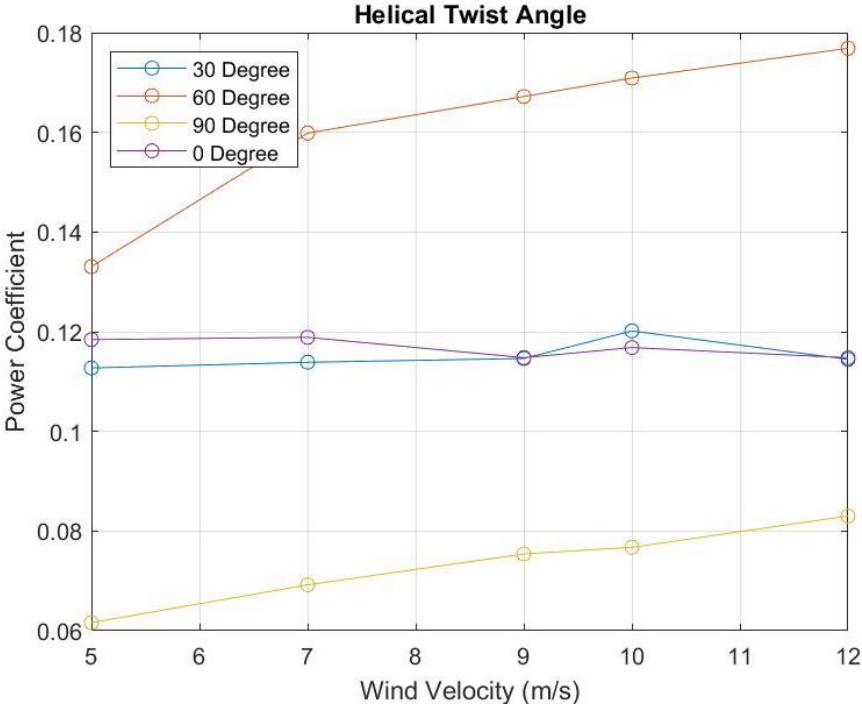
plotted in Figure 12.

FIGURE 12: POWER COEFFICIENT AT DIFFERENT HELICAL ANGLES

Examining the results, 60 degrees had the largest power output of the three designs, therefore,

it provides the optimal angle of twist between the three angles selected. This also confirms the study by

Castelli which also found that 60 degrees was the optimal twist angle for a helical design even compared

to the straight bladed design. [15]

5.2 Final CFD Analysis Setup:

Two models were created, one straight H-type and one helical H-type, with the twist angle of 60°. Figures 13 and 14 below show the models used for this study.
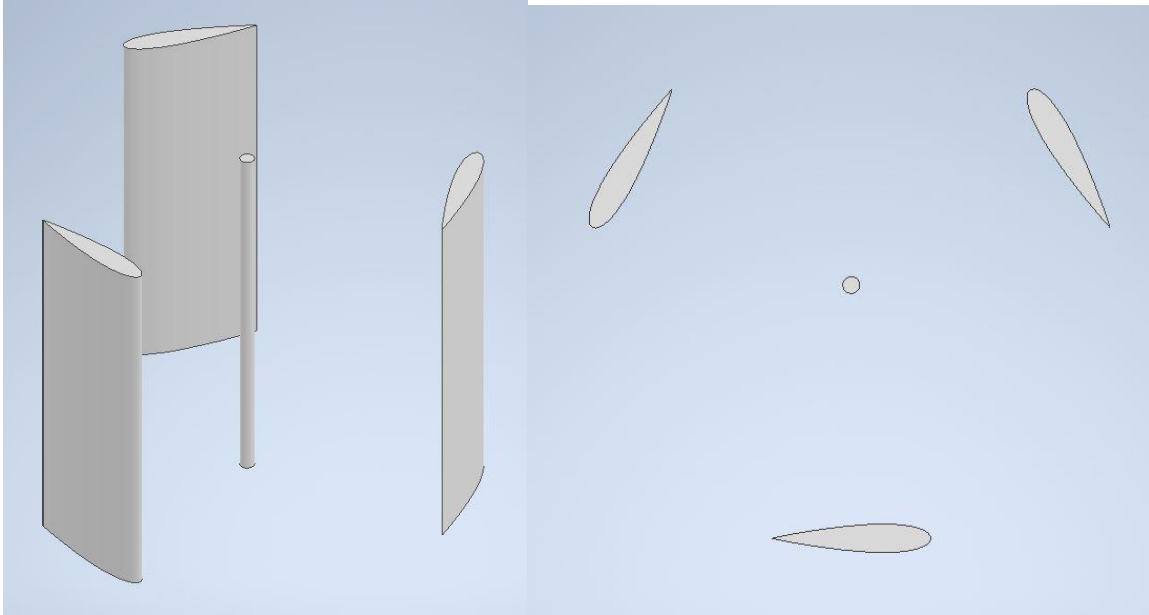
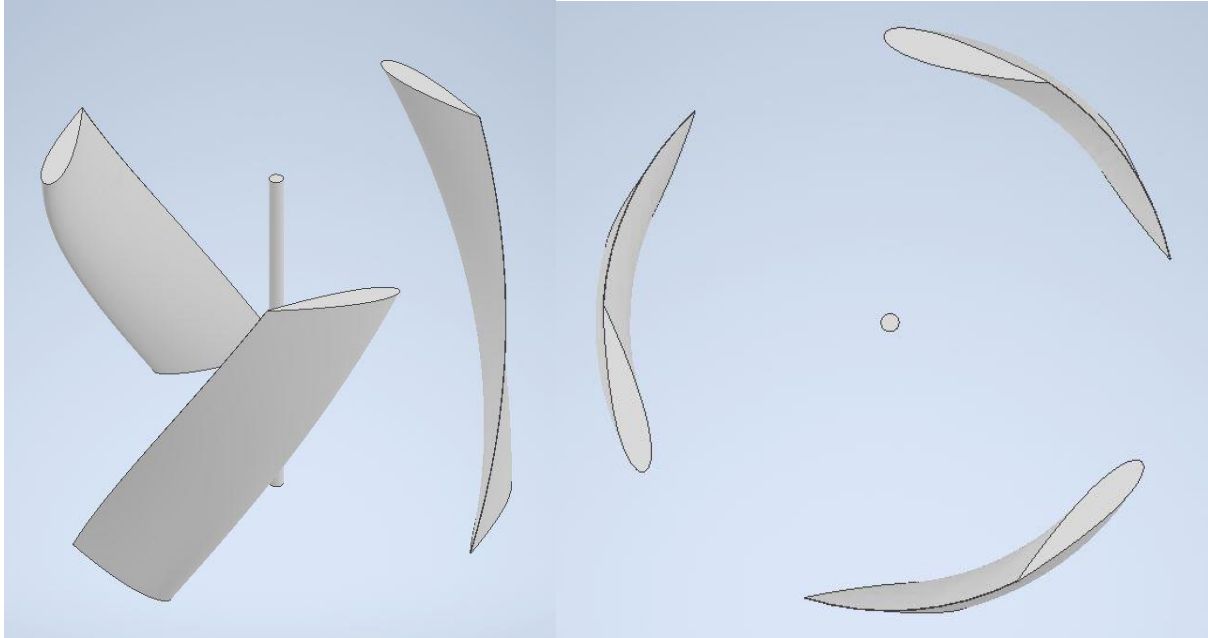**FIGURE 13: STRAIGHT H-TYPE ISO VIEW (LEFT) AND TOP VIEW (RIGHT)**

FIGURE 14: HELICAL H-TYPE ISO VIEW (LEFT) AND TOP VIEW (RIGHT)

Spokes connecting the center shaft and turbine blades were omitted from the simulations because they caused poor accuracy in the results. After a preliminary analysis, the Wall Y+ value, which is a value used evaluate the accuracy of a simulation, was plot on the surface of the turbine and compared a model with spokes and one without.
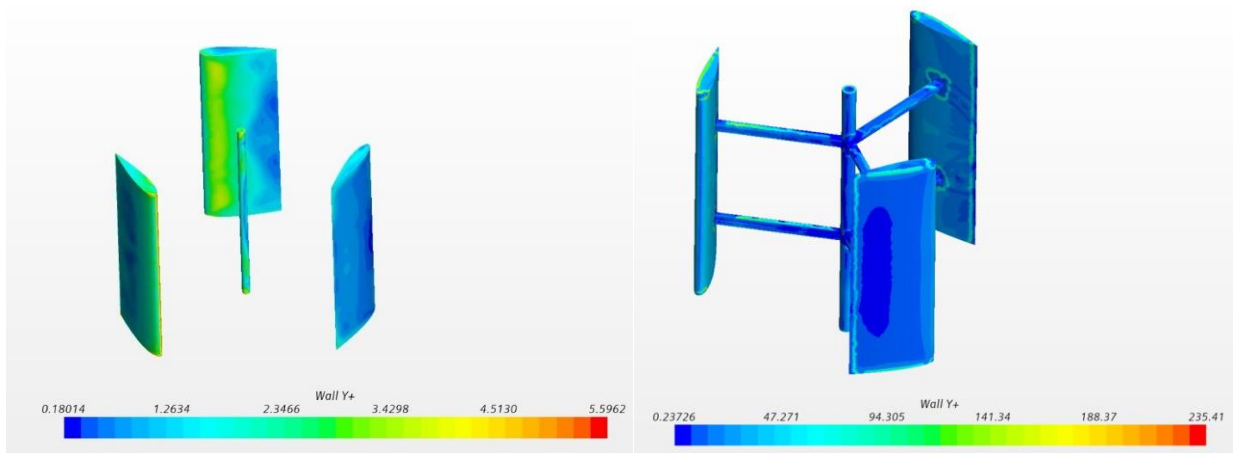
FIGURE 15: SCALAR PLOT OF WALL Y+ OF TURBINE WITH NO SPOKES (LEFT) AND A TURBINE WITH SPOKES (RIGHT)

Figure 15 shows the scalar Wall Y+ surface plots of a turbine with and without spokes, and omitting the spokes placed the range of values from 0 to 5, which is ideal for Wall Y+. Including the spokes greatly increased the Wall Y+ values to over 200 which indicates that the results from this simulation will be very inaccurate. Ideally, this study would like the simulation model and the live wind tunnel model to match; however, the simulations need to have the most accurate results as possible.

5.2.1 Mesh Generation:

A polygonal mesh was chosen for these simulations. Trial simulations were also run for tetrahedral and trimmer meshes; however, polyhedral was found to return the most accurate results and most likely to not diverge. A mesh interface was set for the intersecting faces between the two regions. The following figures detail the mesh used in these simulations.
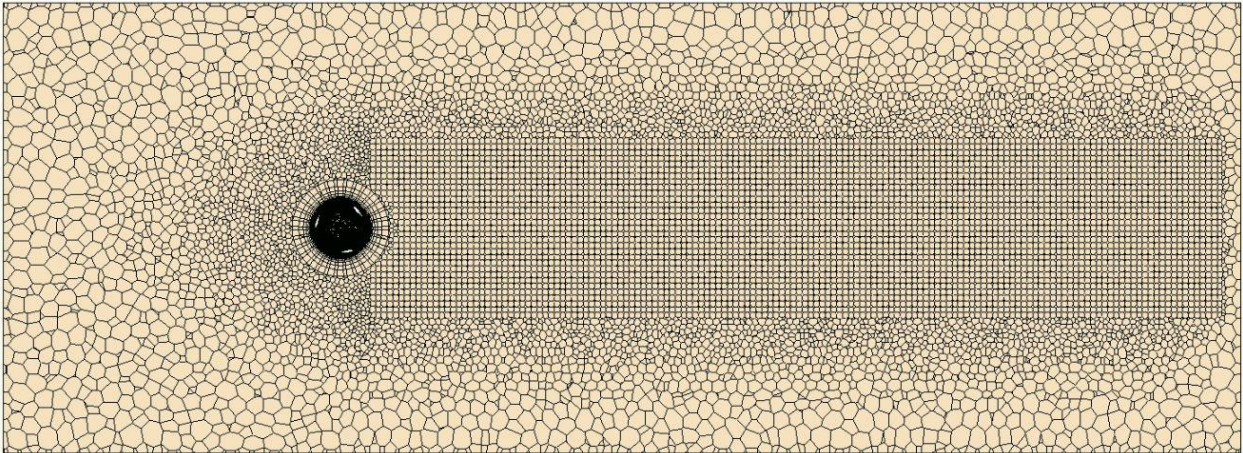

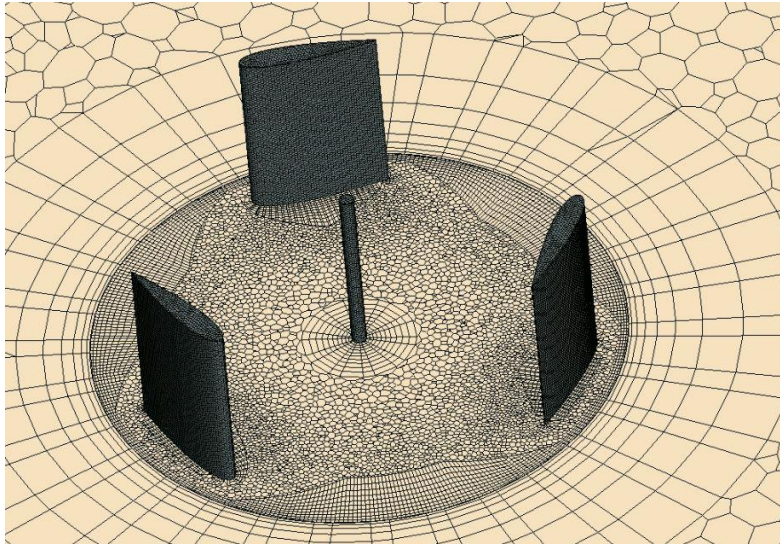**FIGURE 16: TOP SECTION VIEW OF THE MESH**

FIGURE 17: MESH VIEW OF FULL TURBINE

It can be seen from these figures that the area near the turbine and the area past the turbine have a higher density mesh. Not only does this provide a more accurate solution, but it also provides added resolution for examining the wind wake region past the turbine. The turbine models with the mesh are also treated as rigid bodies. Mechanical deflection or vibration were not considered in these simulations. Future research could be done by extracting the forces measured on the turbine surfaces and placing them as inputs for a force analysis; however, this is not covered in the scope of this thesis.

For each test, the inner region was set to the corresponding rotation rate from the given TSR. Similar to the preliminary analysis, the simulations were set to run for a time span of 1 second. A torque measurement was set on the turbine blade boundaries, locating the axis along the center shaft. A line probe was also created, with a beginning point at half the height of the turbine, just past the outer diameter and ending at a distance of 40*R. This probe measured the air velocity past the turbine in order to find the distance at which the air returns to the same uniform inlet air velocity.

6   Wind Tunnel Experiments:

6.1   Experiment Setup:

6.1.1   Wind Tunnel Setup:

The wind tunnel at UWM has three sections: a concentrator section; a test section; and a diffuser section. The concentrator section (or inlet section) has an inlet area of 9.3 m^2 and contracts down at the opposite end by a ratio of 6.2. The inlet contains hexagonal cells to reduce turbulence and allow the air to be as uniform as possible. The test section is where all material related to the experiments are placed. The walls of this section are made of a clear polycarbonate, allowing a clear visual of the entire section while maintaining structural integrity. It also provides a smooth surface to minimize the boundary layer effect as much as possible. The dimensions of this section are 1.2 m x 1.2 m x 2.43 m, and it has a cross sectional area of 1.4 m^2. The last section is the diffuser section, and it expands in area by a ratio of 2.25. This section also houses the six-bladed suction fan with a diameter of 1.83 m that generates the air flow in the tunnel. It is powered by a 25.4 kW motor which is controlled by a variable frequency drive (VFD).

6.1.2   Turbine Test Stand:

Models of the Helical and Straight bladed designs were 3D printed at a 1:1 scale. The center shafts each turbine included a through hole where a threaded rod was fitted, and an epoxy was used to further hold the pieces in place.
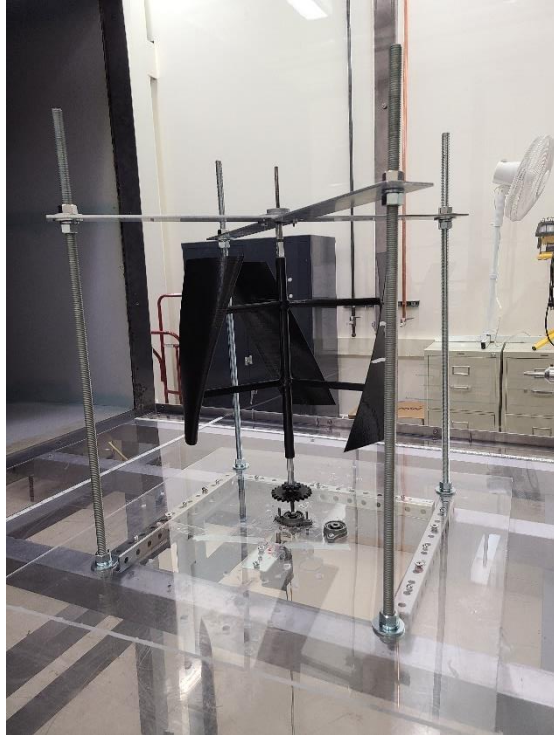
As can be seen from Figure 18, the center shaft is fitted through two ball bearings. The top bearing is

secured to a pair of flat aluminum brackets arranged in a cross shape while the bottom bearing is

secured to the plexiglass base. The brackets are connected by four threaded rods at each end of the

brackets. The bottom of this apparatus is secured to a plexiglass base. Openings in the base are included

to attach the motor and gear system that is used to measure the torque output of the turbine. Once

assembled this entire test stand can be secured to the wind tunnel test section via four screws at the

base.

Measuring the torque of the turbine directly proved to be difficult due to the size the turbine

was restricted to. The torque sensors available to the university's lab were too resistive for the turbine

to turn. The chosen method was one where the torque was measured indirectly. The turbine was first

placed in the wind tunnel with no motor attached. At wind speeds of 5, 7, 9, 10, and 12 m/s, a

tachometer was used to measure the rotation rate of the turbine. Then, a motor is attached to the

turbine using a pair of gears with a 1:1 ratio, and using a DC power supply, power was then transferred

to the motor to turn the turbine. Power was increased until the turbine matched the rotation rate from

each corresponding wind speed, and the applied voltage and current was recorded. These two values

were then used to calculate power.

6.1.3 Wind Velocity and Rotation Rate Measurements

The air velocity in the wind tunnel is controlled by a VFD, and its input parameter is the frequency

for the fan that turns the fan. In order to find the wind velocity to the corresponding input frequency, an

airflow meter was used measure the air velocity at multiple frequencies.

FIGURE 19: IMAGE OF AIRFLOW METER WITH PITOT TUBE ATTACHED

The airflow meter was a Fluke 922 attached to a pitot tube. The pitot tube was placed alone in the wind

tunnel facing the incoming wind. Measurements were recorded from 20 to 44 Hz. These were then

plotted and then a linearization equation was calculated from the data points.
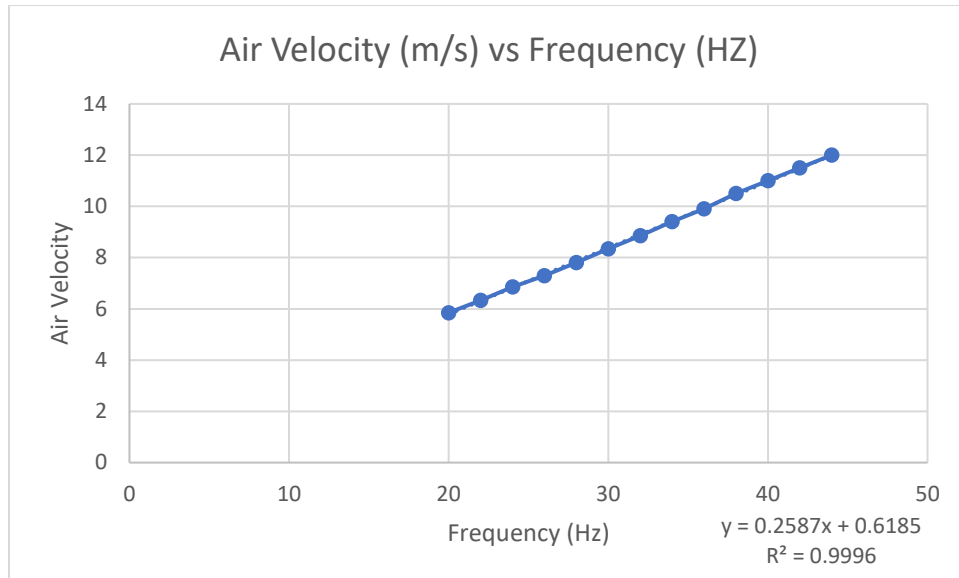
FIGURE 20: PLOT OF AIR VELOCITY VS FREQUENCY OF VFD WITH LINEARIZED EQUATION

Using the equation in Figure 20, the wind tunnel fan could be set to any specific wind velocity needed

for this research.

7   Results and Discussion:

7.1   Turbine Power:

7.1.1 Simulation Results:

The power of the Helical and Straight bladed turbine designs was measured numerically in CFD

simulations using both a LES and RANS style solver. These two physics models provided a more diverse

range of solutions. Figure 21 below details the results of those tests.
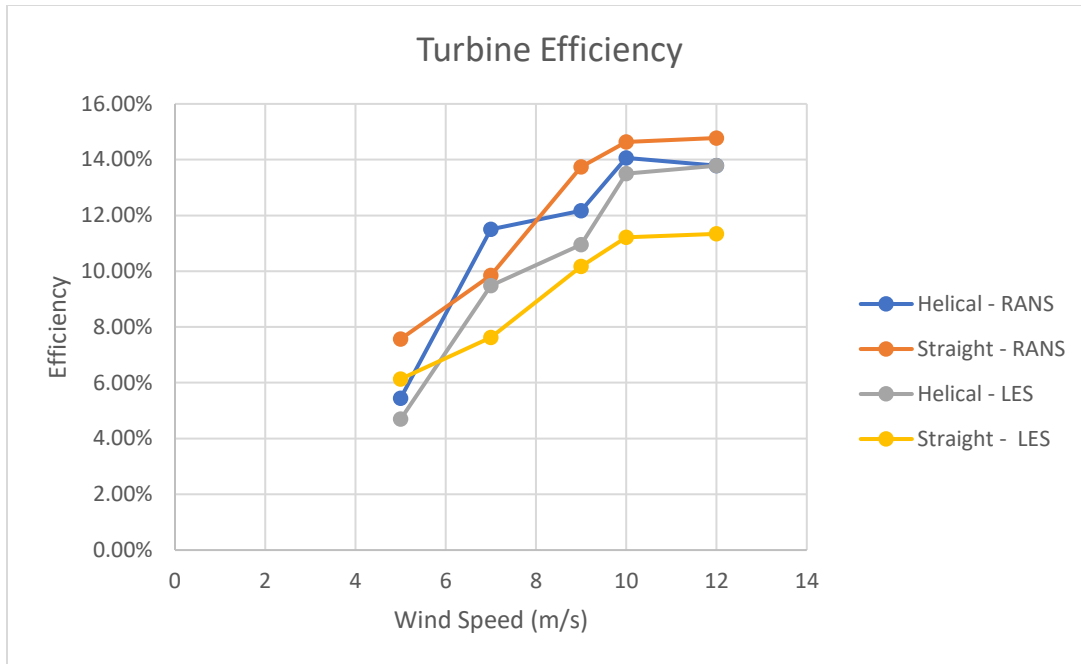
FIGURE 21: POWER OF HELICAL AND STRAIGHT BLADED TURBINES MEASURED EXPERIMENTALLY AND NUMERICALLY.

The LES models show the helical design having a larger power output than the straight bladed design. However, the RANS models show the power output to be nearly equal over this range of wind velocities. At the very least, these results show that the helical design does not lower the power output of the turbine.

7.1.2 Full Scale Turbine:

From these results, a full-scale version of this helical design can be for a target power output. The final power output target is 1 kW. In order to find the required size of the turbine, the following equation is used. (β = H/D)

$$H = \sqrt{\frac{2\beta P_t}{C_p \rho V^3}}$$

(9)

Setting the target power output to 1kW, the air velocity to 10 m/s, and power coefficient to value found in the simulations ($C_p = 0.14$), the final height of the turbine is calculated as 3.15 m. Using this result, the final design has the following parameters:

Full-Scale Design Parameters	
Height	3.15 m
Diameter	3.71 m
Chord	0.371 m
Number of Blades	3

TABLE 2: FULL-SCALE DESIGN PARAMETERS

As stated in the Final Design section, the parameters, such as H/D, set for these test models are likely not the most optimal for a full-scale model. Additional research would be needed to find the best final design. Additionally, the power coefficients found in this research is lower than those found in other studies. Typical Darrieus VAWTs had power coefficients in the range of 0.3 to 0.4. This discrepancy is likely because of the small scale of the turbines used in this research. Most other studies used full scale simulations; however, this research was limited by the size of the wind tunnel test section. When creating a full-scale design, some physical design points must also be considered, such as weight, material, and structural stability.

7.2 Starting Torque:

Starting torque is the minimum torque needed to begin turning the turbine from a resting position. Darrieus turbines have been found to have poor self-starting capabilities, meaning they typically need an outside force to get them to begin rotating. They cannot begin to rotate on their own. Helical turbines can begin to rotate on their own. To test when the turbines begin to rotate, each design was placed in the wind tunnel and the wind speed was incrementally increased until the turbine began to completely rotate and continuously rotate. However, it was found that the self-starting capabilities of

each design heavily relied on the position of the turbine blades relative to the incoming wind. Therefore, there were four designated starting blade positions.
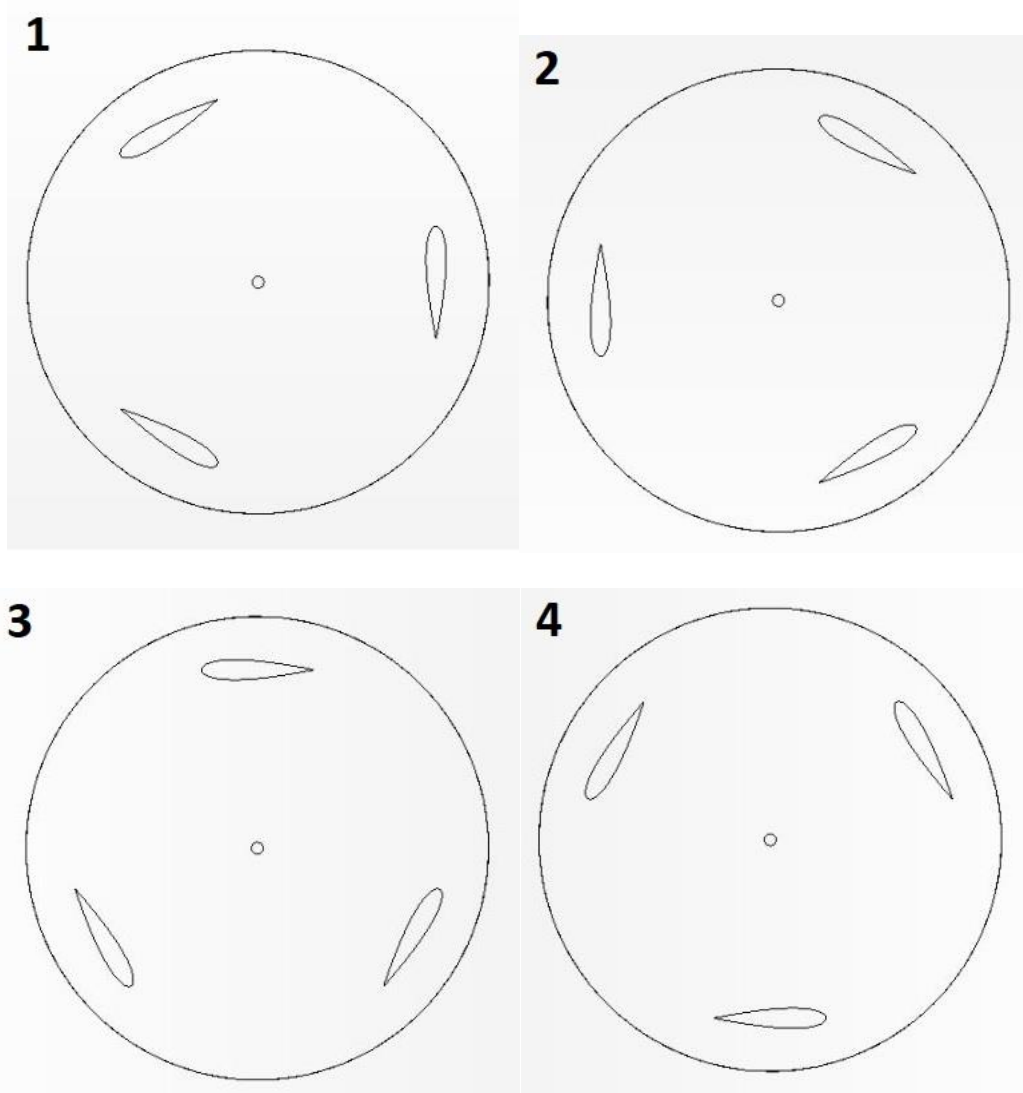
FIGURE 22: STARTING POSITIONS FOR THE TURBINE BLADES IN THE SELF-STARTING TEST

These images show a cross section of the blades viewed from above the turbine. Since in the helical design, the cross section of the blades rotates around the center axis, the starting position was made in reference to the center cross section of the turbine. The starting torque was found for each design at each blade position. Table 3 details the results.

Starting Torque Test		
	Starting Wind Speed (m/s)	
Position	Helical	Straight
1	3	5
2	X	X
3	5	X
4	3	5

TABLE 3: TABLE OF STARTING TORQUE TEST RESULTS

The first notable result is that each design failed to self-start when the blades when placed in position 2.

In addition, the straight bladed design also failed to self-start at position 3. The helical design was able

to self-start at lower wind speeds at positions 1 and 4.

As discussed in the power output tests results, the torque of a vertical axis turbine oscillates as

the blades rotate around the axis. Therefore, the forces experienced by the blades have a maximum and

minimum at specific locations. The self-starting test shows how position 2 is where the minimum torque

values are experienced by the turbine, while the maximum is experienced at position 1. In order for the

turbine to rotate, one side of the turbine needs to produce a stronger tangential force than the opposite

side. In their study on the starting torque of a Darrieus wind turbine, M. Douak illustrates the normal

and tangential forces experienced by a turbine blade at each position around the center axis. [20]
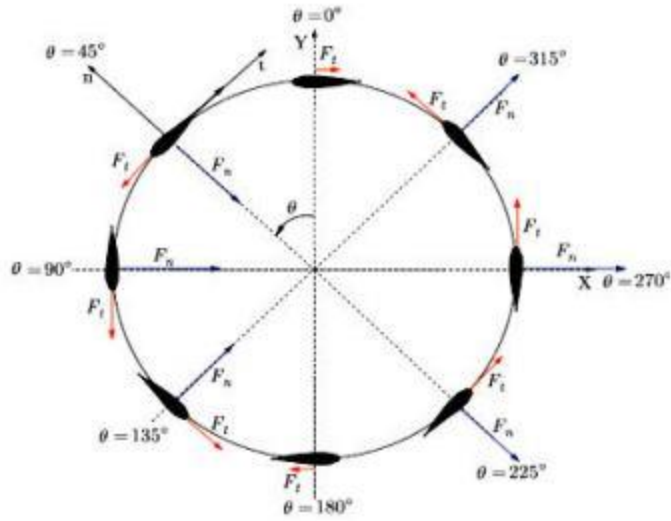
FIGURE 23: DIAGRAM OF NORMAL AND TANGENTIAL FORCES IN A TURBINE BLADE
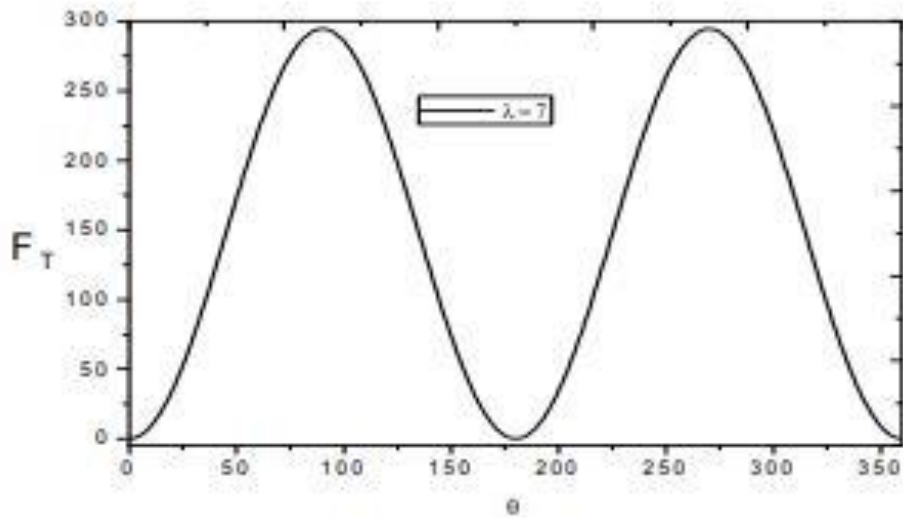
FIGURE 24: PLOT OF TANGENTIAL FORCES OF TURBINE BLADES [20]

Figure 24 shows how the tangential forces, starting from θ = 0°, increase to a maximum at θ = 90° and then return to a minimum at θ = 180°. And then same behavior occurs between θ = 180° and 360°. Examining the normal forces of the blade, there is a large maximum at θ = 90°, and as opposed to the tangential forces, there is a considerably smaller peak in the second half of the rotation. The positive tangential force is what drives the rotation of the turbine while it opposes the smaller normal forces in the downstream side of the semi-circle.

Comparing this to the self-starting test, Figure 25 illustrates why each turbine design would not rotate at position 2, which corresponds to θ = 90° in Figure 23. At this position the opposing force that prevents the turbine from rotate is at its greatest. The straight bladed turbine was also unable to rotate from position 3 as well. Notably, during the test at position 3, the blades would slightly rotate in the reverse direction and then stop in position 2. The helical turbine was able to self-start from position 3; however, it required a large wind velocity than the other two positions.

Using the CFD simulations, the forces on each were extracted and plotted in a similar way to Figures 24 and 25. Star CCM+ uses a cartesian coordinate system so the forces in the X, Y, and Z directions were measured for each blade then these values could be converted to normal and tangential

34

coordinate system. In this case only the X and Z directions were relevant as the Y direction was the axis that ran along the center axis of the turbine.
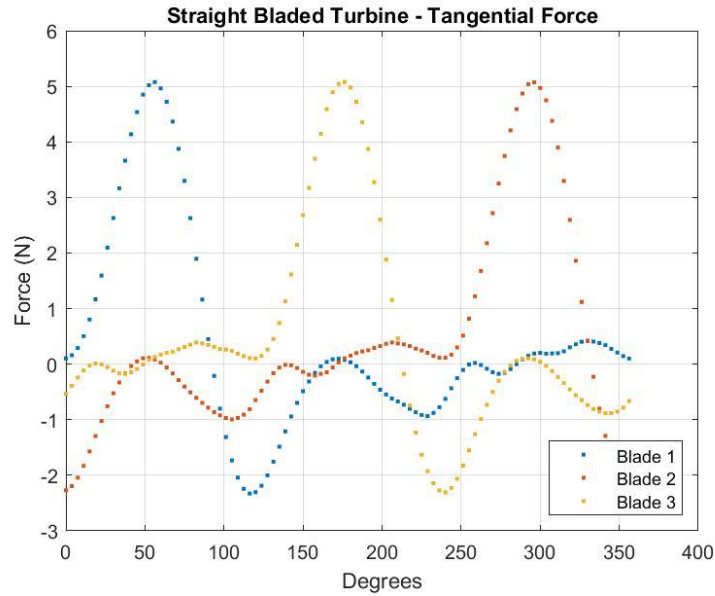

FIGURE 26: TANGENTIAL FORCES IN EACH BLADE FOR STRAIGHT BLADED TURBINE
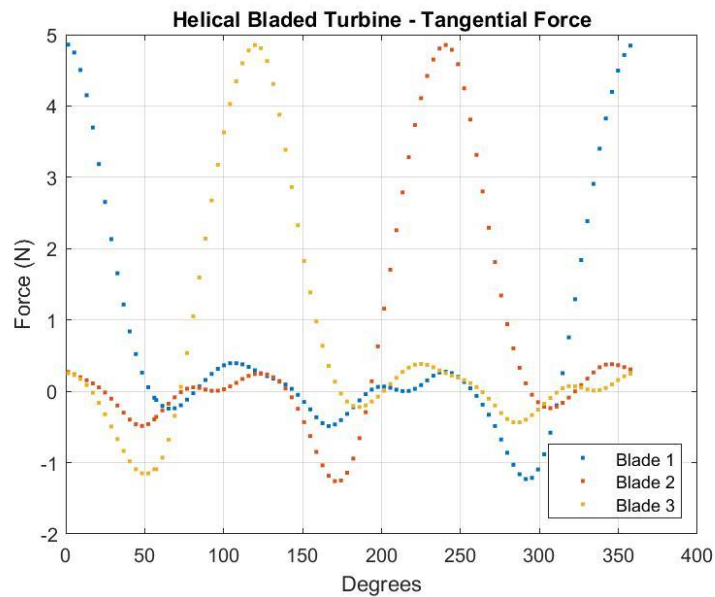

FIGURE 27: TANGENTIAL FORCE IN EACH BLADE FOR HELICAL BLADED TURBINE

Figures 26 and 27 plot the tangential forces in each blade for both turbine designs. Both plots show the same pattern of three lines having the same trend and amplitude but offset by 120 degrees. This is expected as each blade is separated by 120 degrees around the center axis.
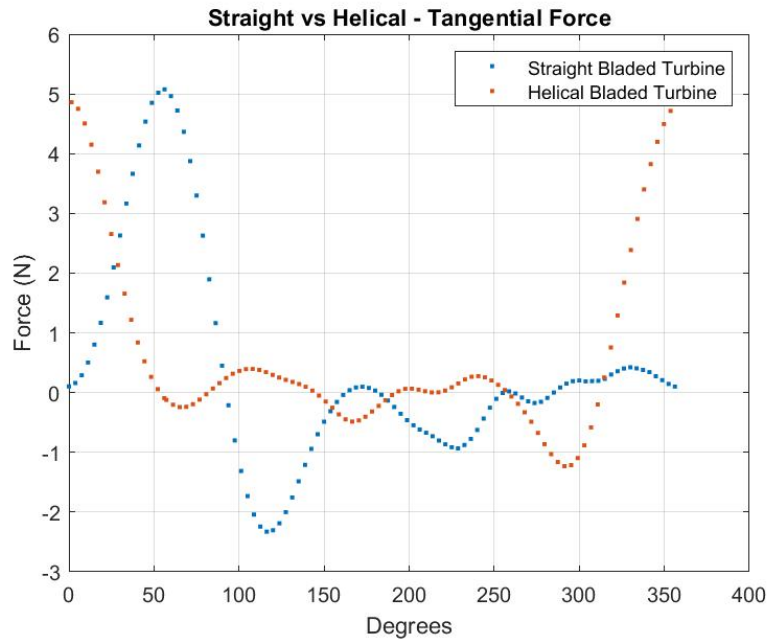
FIGURE 28: STRAIGHT VS HELICAL BLADED TURBINE TANGENTIAL FORCE OF BLADE 1

Figure 28 compares the tangential force of a single blade for the Straight bladed and Helical bladed designs. Both plots have a similar pattern where there is a positive peak immediately followed by a negative peak and then several small peaks that return to around zero. Firstly, this is much different than the plot in Figure 24 which shows a perfectly sinusoidal curve with two large peaks at 90 and 270 degrees of equal magnitude. In Figure 28 the second peak does not return to the same value as the first peak. The plots from Douak were created using theoretical equations for force in a Darrieus turbine blade and thus represent an ideal case, while this study used measured results from a simulation. Examining Figure 28 further, the straight bladed turbine had a high initial peak followed a lower magnitude negative peak, while the helical design had a near equally high initial peak but a much

36

smaller negative peak. The peak of the helical design also occurs about 50° ahead sooner than the

straight bladed turbine.

The plots for normal force in the blades tell a similar story.
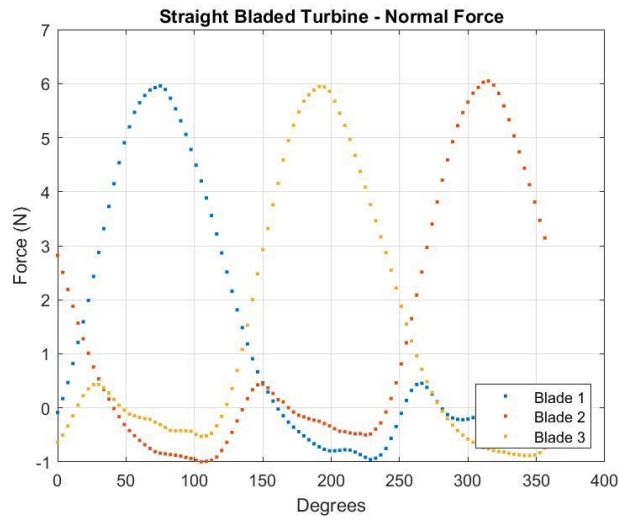

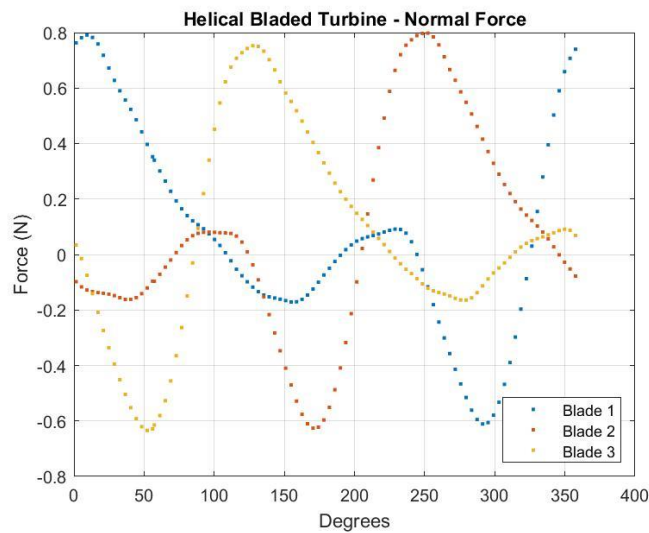FIGURE 29: NORMAL FORCE IN THE BLADES OF THE STRAIGHT BLADED TURBINE

FIGURE 30: NORMAL FORCE IN THE BLADES OF THE HELICAL BLADED TURBINE

In Figures 29 and 30 the normal forces of the turbine follow a similar pattern that is also separated by
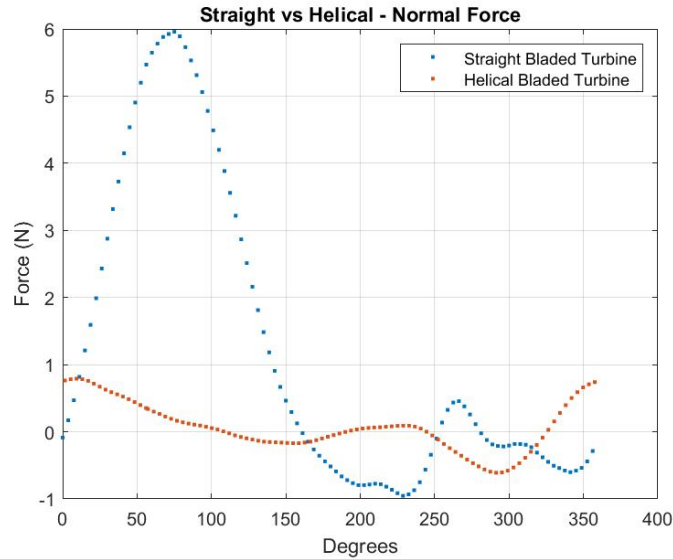
120 degrees.

FIGURE 31: STRAIGHT VS HELICAL BLADED TURBINE NORMAL FORCE OF BLADE 1

Figure 31 plots the first blade of each turbine design, and this pattern is very similar to the normal force

plot from Douak. There is an initial peak around 90 degrees that trails down to zero on the second half

of the blade's rotation. Notably the normal force peak in the helical design is much smaller than the

straight bladed design, which indicates the resistance that the blades need to overcome in order to

rotate is smaller in the helical design. A smaller normal force relative to the tangential force

demonstrates why the helical turbine performs better at self-starting than the straight bladed design.

7.3   Wake Region Analysis:

7.3.1   Uniform Flow Recovery:

Velocity recovery is an important characteristic for a wind turbine, especially in a situation

where there is an array or farm of many turbines stationed together. It can determine how far the

turbines need to be stationed from each to not diminish the power output caused turbulence from a

nearby turbine. Using the results of the CFD simulations, the velocity fields in the wake of the turbine

can be extracted to find the distance at which the velocity field returns to uniform flow. Figure 32 and

Figure 33 depict the velocity fields of the simulation domain along a sectional plane cutting across the

center of the helical and straight bladed turbines. The image illustrates how the turbine disturbs the

uniform inlet airflow and how the air recovers back to that uniform flow.
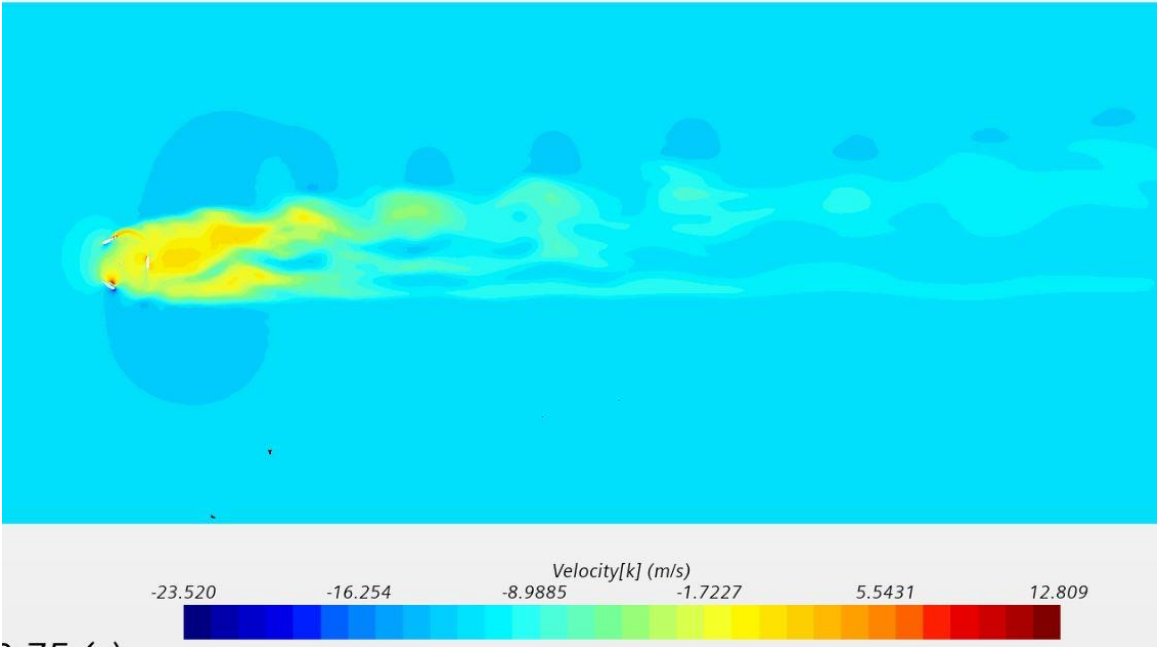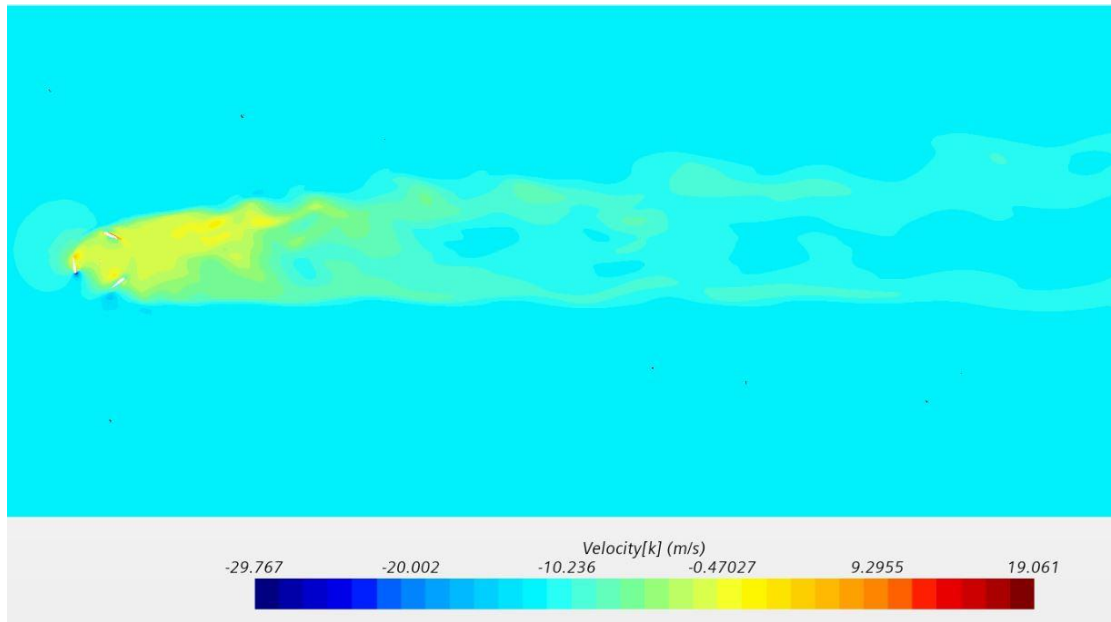

FIGURE 32: VELOCITY FIELD OF HELICAL BLADED TURBINE

FIGURE 33: VELOCITY FIELD OF STRAIGHT BLADED TURBINE

Both images show a similar pattern of the shifting slightly upward, relative to the orientation of the image. This is understandable considering the turbines are rotating clockwise from the view of these images; therefore, the disturbances caused by the blades will direct the air in that direction as it flows through the turbine. Notably, the disturbances along the lower rotating edge of each turbine are generally less turbulent and act more as a strip as it recovers to uniform flow.

Velocity recovery will be defined as the distance from the turbine from which the airflow returns to uniform flow equal to the inlet air velocity. The distance will be defined as the ratio between the exact distance from last rotating edge of the turbine to the diameter of the turbine. (x/D) The velocity recovery is defined as the ratio of the air velocity to the velocity of the inlet airflow.
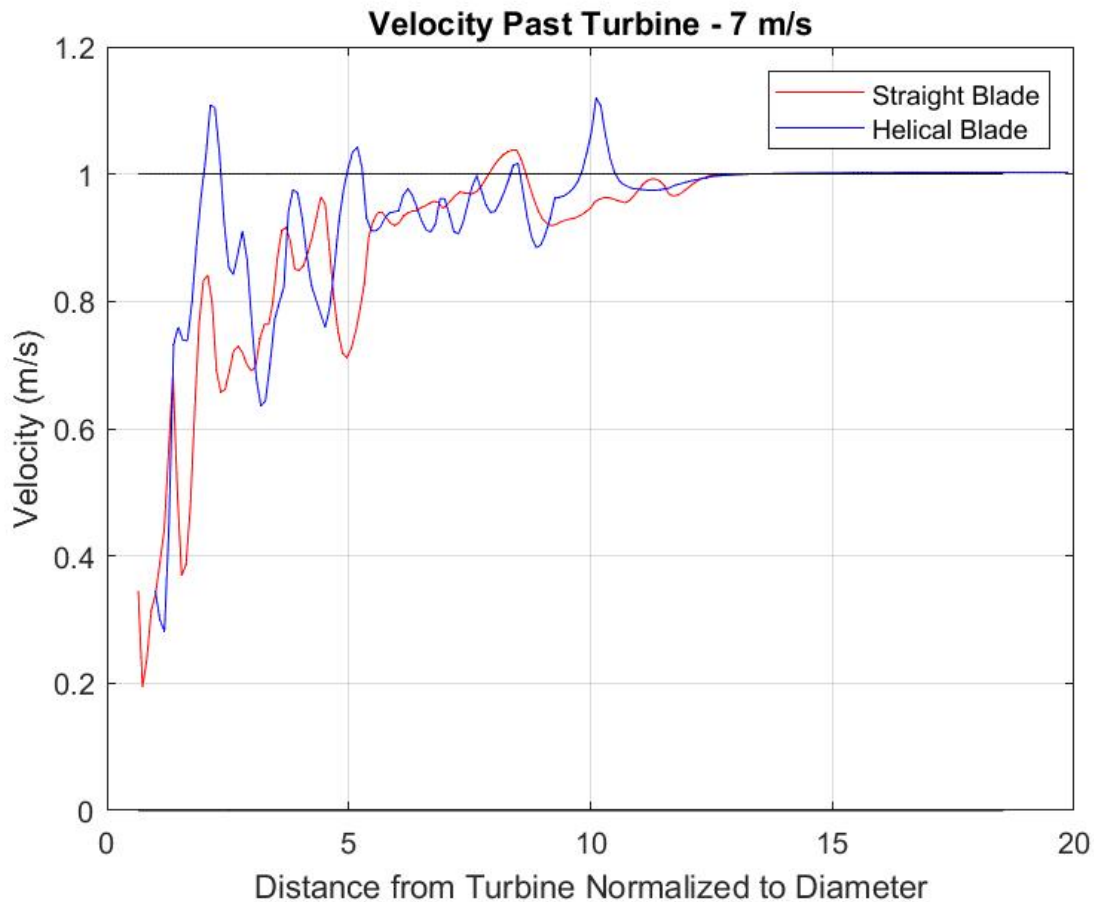
FIGURE 34: VELOCITY RECOVERY IN THE WAKE REGION FOR HELICAL AND STRAIGHT BLADE DESIGNS

Figure 34 illustrated the air velocity past each turbine design at 7 m/s. The velocities for both designs

recover to uniform flow at nearly the same location of 13D. The remaining plots are in Appendix A. Each

design was evaluated at the same five air velocities, and each plot showed the same trend of the air

velocities recovering to uniform flow at the same distance. Thus, the helical design did not show

evidence of improving air velocity recovery compared to the Darrieus straight bladed design.

In order a more complete picture of the velocity recovery, plane section views of the velocity

fields were extracted from the simulations. Sections were created at distances of 1D, 3D, and 5D. The air

velocity was also normalized to the input air velocity.

41
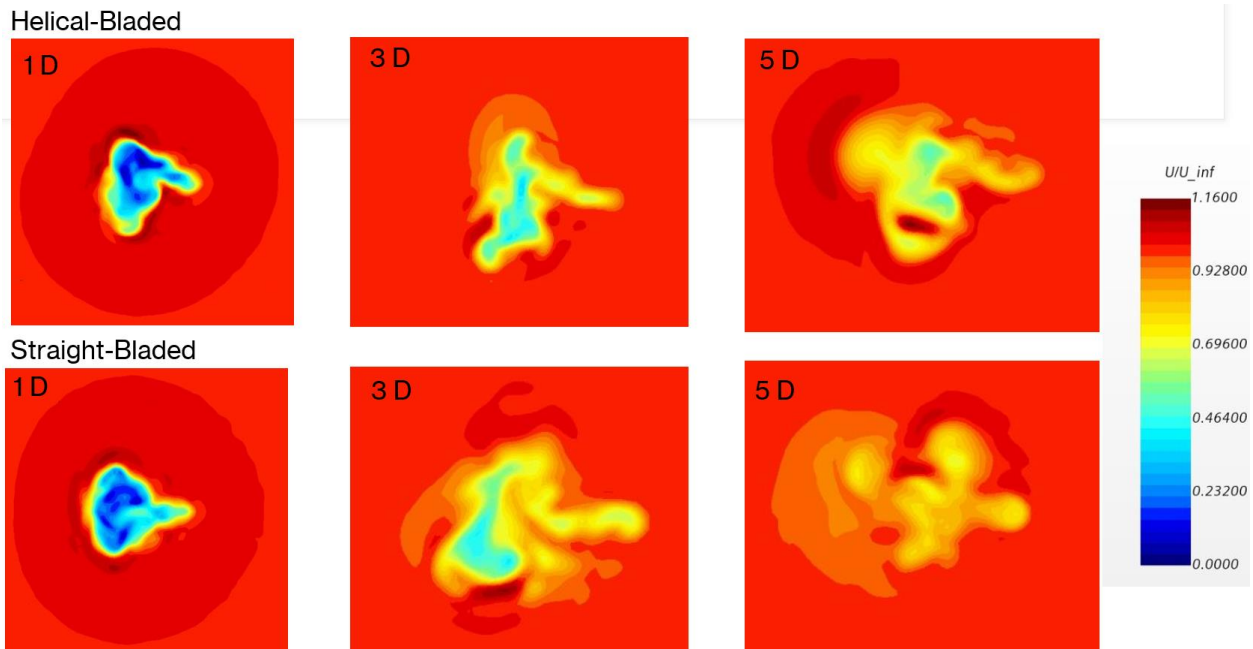
FIGURE 35: PLANE SECTIONS OF THE VELOCITY FIELDS PAST THE HELICAL BLADED AND STRAIGHT BLADED TURBINES FOR 12 M/S

Figure 35 compares the velocity fields of the helical and straight bladed designs at 12 m/s. The airflows have similar progressions, and there is little difference in the amount of dissipation between the two designs. The evidence would then suggest that a 60° helical angle has marginal benefits for velocity recovery. This pattern is found at every inlet velocity as well. Their plots can be found in Appendix C. From the findings by Divakaran, it can be inferred that the velocity recovery would improve has the helical angle continues to increase; however, there will be a decrease in power output. Considering these type of turbine designs will be used as stand-alone or small-scale settings with already turbulent air, velocity recovery is the least important characteristic of a VAWT turbine.

7.3.2 Wake Region Turbulence:

To evaluate turbulence in the wake region of each turbine, the value turbulent viscosity was extracted on a planar section of the simulation domain. The section is a horizontal slice from the center of the

42

turbine and gives a top-down view. Turbulent viscosity is a measure of the turbulent transfer of energy due to moving eddies.
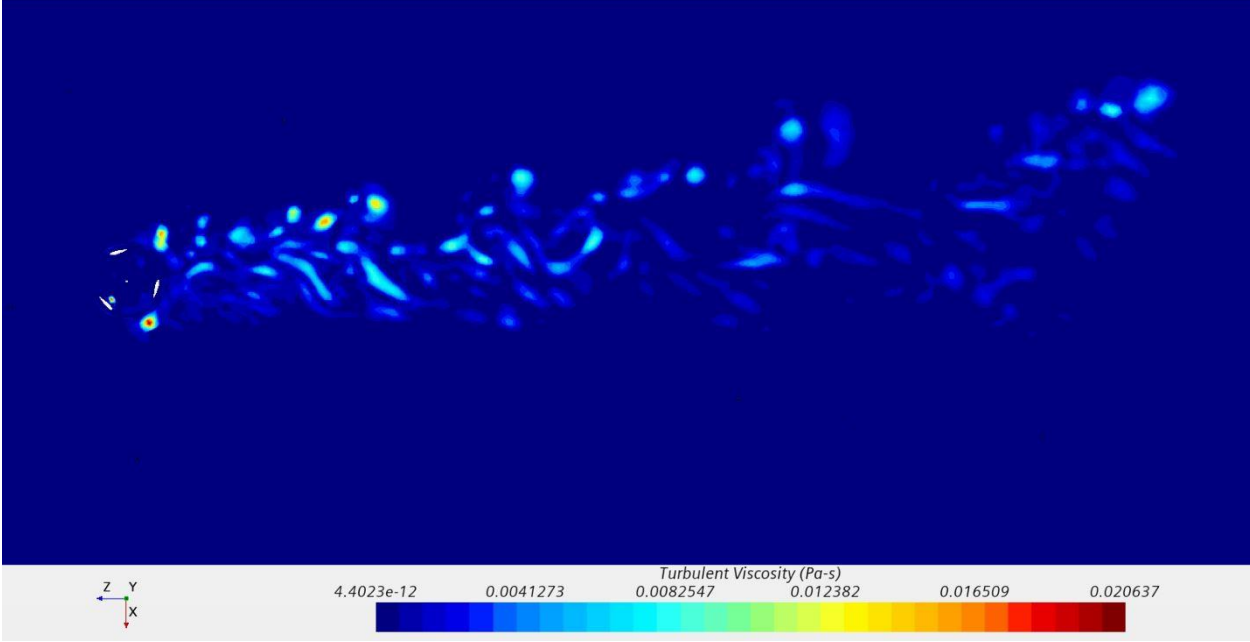
FIGURE 36: TURBULENT VISCOSITY FIELD OF SIMULATION DOMAIN FOR THE STRAIGHT BLADED DESIGN AT 12 M/S
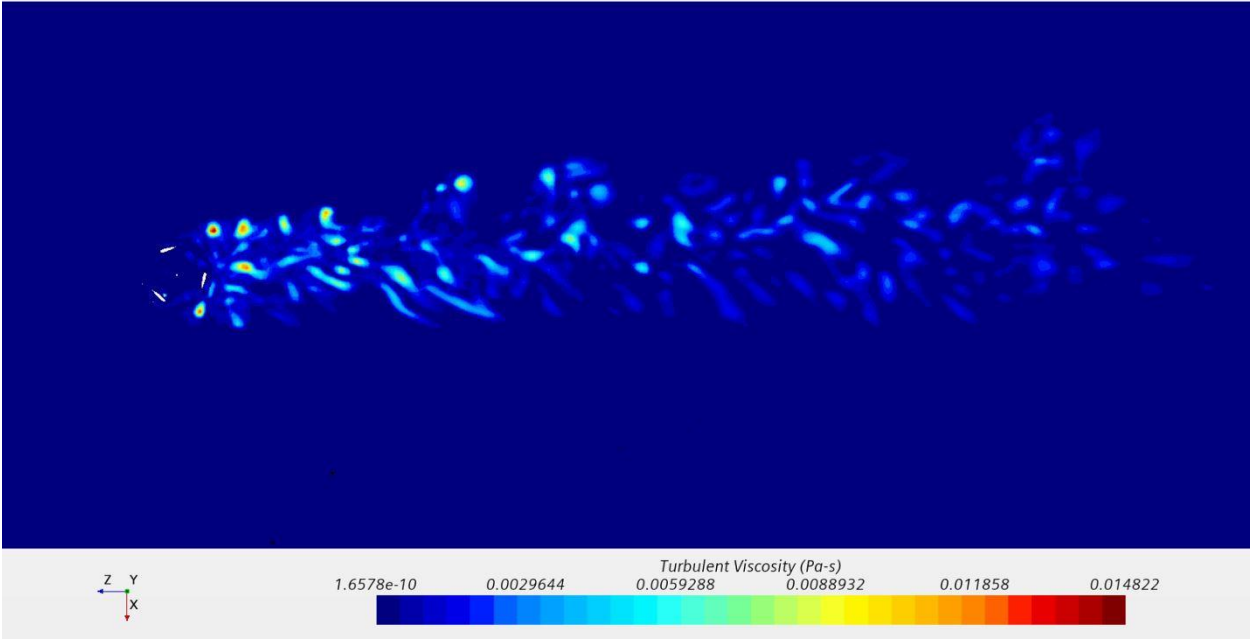

FIGURE 37: TURBULENT VISCOSITY OF SIMULATION DOMAIN FOR THE HELICAL BLADED DESIGN AT 12 M/S

Figures 36 and 37 depict the turbulent viscosity in the wake region for turbine designs at 12 m/s. Both

designs have a similar flow field, but the helical design had a small maximum value of turbulent

viscosity. Flow fields for each design at each inlet velocity are listed in Appendix B. The following table

compiles the maximum viscosity values from each case.

Turbulent Viscosity Maximum (Pa-s)		
Velocity (m/s)	Helical	Straight
5	0.0095711	0.0094477
7	0.0092293	0.0099546
9	0.01295	0.015277
10	0.013824	0.012226
12	0.014822	0.020637

TABLE 4: TABLE OF MAXIMUM TURBULENT VISCOSITY VALUES FOR EACH TURBINE DESIGN

Overall, the helical design had a slight improvement in turbulent viscosity in the wake region. The most

important characteristic that can be inferred from the wake turbulence is the noise generated by the

turbine. Since these types of turbines are designed for residential use, they must minimize the amount

of disturbance they have on its environment. According to these results, a 60° helical angle provides

marginal improvement in the turbulences generated by the turbine. Similar to the previous section, it is

likely that increasing the helical will continue to improve the wake turbulence, and therefore noise.

However, again this would sacrifice the amount of power generated by the turbine.

7.3.3   Torque Fluctuation:

Torque fluctuation is a measure of the change in torque experienced in the turbine shaft as it rotates.

This characteristic can be a source for mechanical vibrations in the turbine, which are a factor in the

fatigue life of the design. From the CFD simulations, the torque fluctuation coefficient was calculated for

the last revolution of each design at each wind velocity, and Figure 38 compared the two designs at each
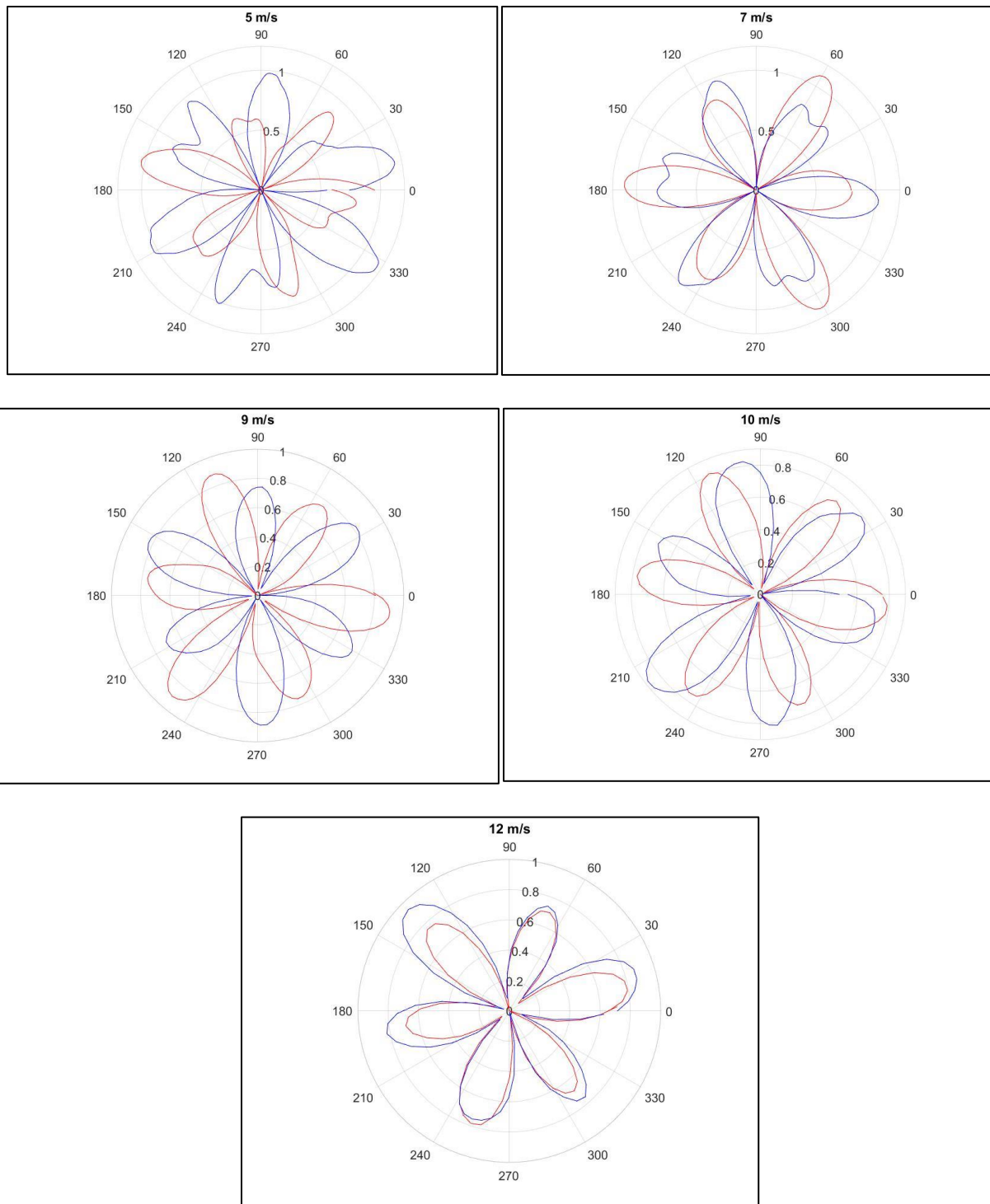
speed.

These polar plots show how each design follow similar patterns of fluctuation. At some points, such as

for 9 and 10 m/s, the patterns are nearly identical, except shifted about 5 to 10 degrees. The fluctuation

45

patterns for the Straight bladed design seem to be more erratic at the lower wind speeds, and patterns for both designs smooth out as the wind speed and rotation rate increase. Ultimately the helical design did not show evidence of improving the torque fluctuation.

8 Conclusion:

The goal of this thesis was to determine if adding a helical twist to a Darrieus vertical axis wind turbine improves the design in any quantifiable characteristics. Ultimately, it improved the self-starting capabilities and the power output, which are two of the most important factors of a VAWT. Power output was measured in both wind tunnel tests and in numerical simulations in Star CCM+, and the helical design was shown to have a higher power output for a helical angle of 60°. From there, as the helical angle is increased, the power output begins to decrease. The helical design also showed significantly better self-starting capabilities, which is an improvement from the Darrieus turbine's notable inability to self-start. The CFD analysis found no evidence that the 60° helical design improved velocity recovery or torque fluctuation. Lastly, there was a slight improvement in the turbulence produced in the wake region for the helical design, which indicates there is less noise generated by the turbine. Overall, the helical VAWT design was shown to have better qualities than the straight bladed Darrieus VAWT design, specifically in power output and self-starting ability.

9 References

[1] Intergovernmental Panel on Climate Change, "Climate Change 2021: The Physical Science Basis. Contribution of Working Group I to the Sixth," Cambridge University Press. In Press, 2021.

[2] U.S. Department of Energy Office of Energy Efficiency and Renewable Energy, "Land-Based Wind Market Report: 2021 Edition," 2021.

[3] U.S. Department of Energy Office of Energy Efficiency and Renewable Energy, "Offshore Wind Market Report: 2021 Edition," 2021.

[4] US Department of Energy Office of Energy Efficiency and Renewable Energy, "Distributed Wind Market Report: 2021 Edition," 2021.

[5] A. Mills, R. Wiser and K. Porter, "The Cost of Transmission for Wind Energy: A Review of Transmission Planning Studies," Ernest Orlando Lawrence Berkeley National Laboratory, 2009.

[6] M. Kumar, K. Sivalingam and T.-C. Lim, "Strategies for Enhancing the Low Wind Speed Performance of H-Darries Wind Turbine," *Clean Technologies,* vol. 1, pp. 185-204, 2019.

[7] G. J. M. Darrieus, "Turbine Having its Rotating Shaft Transverse to the Flow of the Current". US Patent 1,835,018, 12 August 1931.

[8] L. Bastisti, A. Brighenti, E. Benini and M. R. Castelli, "Analysis of Different Blade Architechtures on Small VAWT Performance," *Journal of Physics: Conference Series,* 2016.

[9] A. Gorlov, "Development of the Helical Reaction Hydraulic Turbine," US Department of Energy, Washington, DC, 1998.

[10] J. Baker, "Features to Aid or Enable Self Starting of Fixed Pitch Low Solidity Vertical Axis Wind Turbines," *J. Wind Eng. Ind. Aerodyn,* vol. 15, pp. 369-380, 1983.

[11] B. Blackwell and G. Reis, "Blade Shape for a Troposkein Type of Vertical Axis Wind Turbine," Sandia Labs, Albuquerque, NM, 1974.

[12] M. Shiono, K. Suzuki and S. Kiho, "Output Characteristics of Darrieus Water Turbine with Helical Blades for Tidal Current Generation," *International Offshore and Polar Engineering Conference,* 2002.

[13] U. Divakaran, A. Ramesh, A. Moammad and R. K. Velamati, "Effect of Helix Angle on the Performance of Helical Vertical Axis Wind Turbine," *Multidisciplinary Digital Publishing Institute,* vol. 14, 2021.

[14] Q. Cheng, X. Liu, H. S. Ji, K. C. Kim and B. Yang, "Aerodynamic Analysis of a Helical Vertical Axis Wind Turbine," *Energies,* vol. 10, no. 4, p. 575, 2017.

[15] M. R. Castelli, S. D. Betta and E. Benini, "Effect of Blade Number on a Straight-Bladed Vertical-Axis Darrieus Wind Turbine," *International Journal of Aerospace and Mechanical Engineering,* 2012.

[16] Y.-T. Lee and H.-C. Lim, "Numerical Study of the Aerodynamic Performance of a 500W Darrieus-Type Vertical-Axis Wind Turbine," *Renewable Energy: An International Journal,* 2015.

[17] F. N. Modi and N. R. Gilke, "Computational Analysis of Various Airfoil Profile on the Performance of H-Darrieus Wind Turbine," *2018 IEE International Conference on System, Computation, Automation and Networking (ICSCAN),* vol. 10, pp. 1-5, 2018.

[18] A. Bianchini, "Design Guidlines for H-Darrieus Wind Turbines: Optimization of the Annual Energy Yield," *Energy Conversion and Management,* 2014.

[19] B. Sanders, S. Vander Pijl and B. Koren, "Review of Computational Fluid Dynamics for Wind Turbine Wake Aerodynamics," *Wind Energy,* vol. 14, pp. 799-819, 2011.

[20] Z. A. M. Douak, "Starting Torque Study of Darrieus Wind Turbine," *World Academy of Science, Engineering and Technology International Journal of Physical and Mathematical Sciences,* vol. 9, no. 8, 2015.

[21] N. J. Wei, I. D. Brownstein, J. L. Cardona, M. F. Howland and J. O. Dabiri, "Near-Wake Structure of Full-Scale Vertical Axis Wind Turbines," *Journal of Fluid Mechanics,* 2021.

[22] S. Joo, H. Choi and J. Lee, "Aerodynamic Characteristics of Two-Bladed H-Darrieus at Various Solidities and Rotating Speeds," *Energy,* vol. 90, pp. 439 - 451, 2015.

[23] N. Franchina, O. Kousaissah, G. Persico and M. Savini, "Three-Dimensional CFD Simulation and Experimental Assessment of the Performance of a H-Shape Vertical Axis Wind Turbine at Design and Off-Design Conditions," *International Journal of Turbomachinery Propulsion and Power,* vol. 4, no. 30, 2019.

[24] *Probes for hot wire anemometry,* Skovlunde, Denmark: Dantec Dynamics, 2014.

[25] *Installation and user's guide for mini CTA 54T30,* Skovlunde, Denmark: Dantec Dynamics, 2004.

[26] *User's guide for hot wire calibrator 54H10,* Skovlunde, Denmark: Dantec Dynamics, 2003.

[27] S. M. A. Jazuli Fadil, "Performance Comparison of Vertical Axis and Horizontal Axis Wind Turbines to Get Optimum Power Output," *15th International Conference on Quality in Research (Q/R): International Sympossium on Electrical and Computer Engineering,* pp. 429-433, 2017.

[28] D. Han, "Design, Fabrication, and Performance Test of a 100-W Helical-Blade Vertical-Axis Wind Turbine at Low Tip-Speed Ratio," *Energies,* vol. 11, no. 6, p. 1517, 2018.
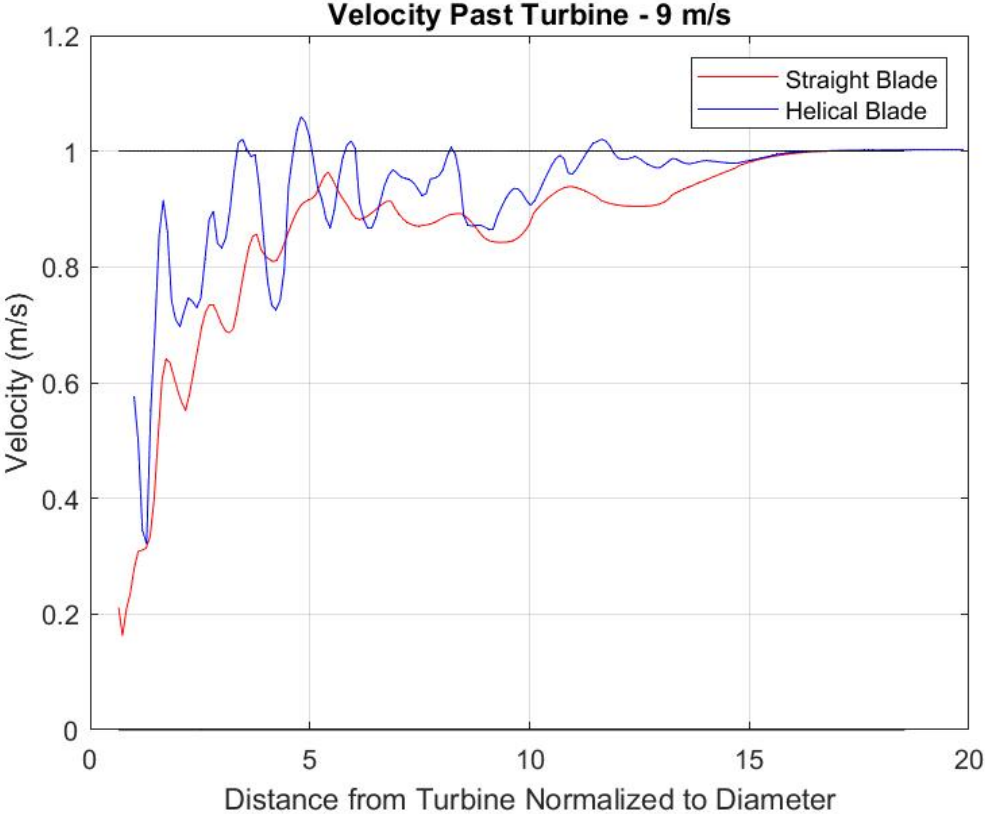
10 Appendix A:

(1): Velocity Recovery Plot for helical and straight blade designs at 5 m/s.

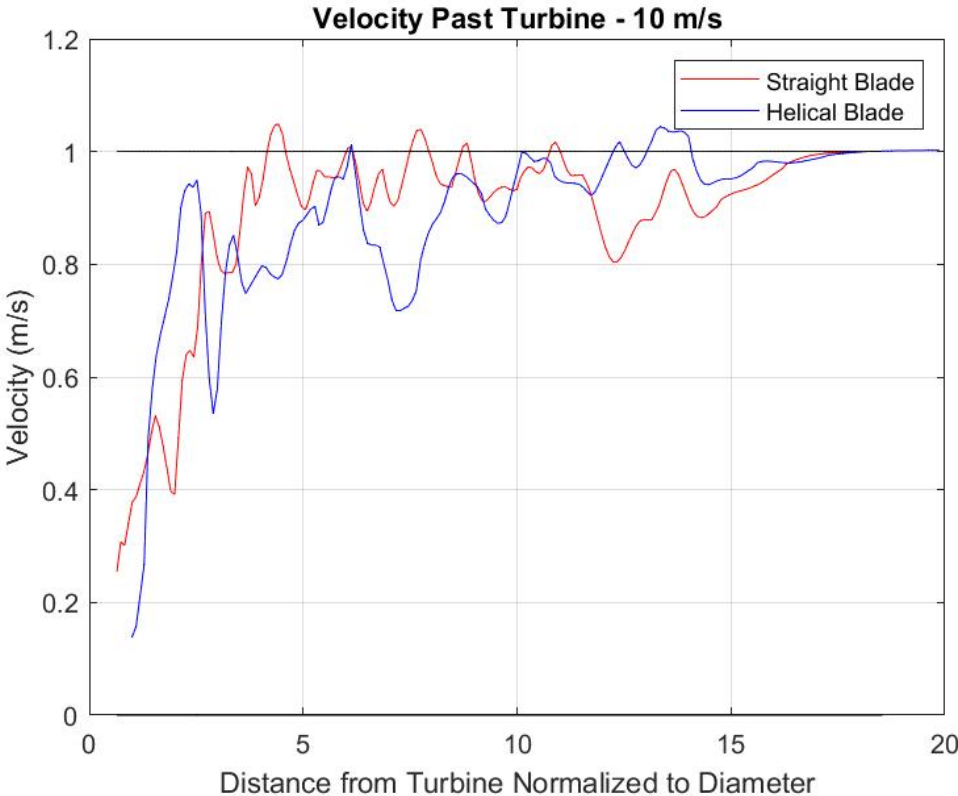**Velocity Past Turbine - 5 m/s**
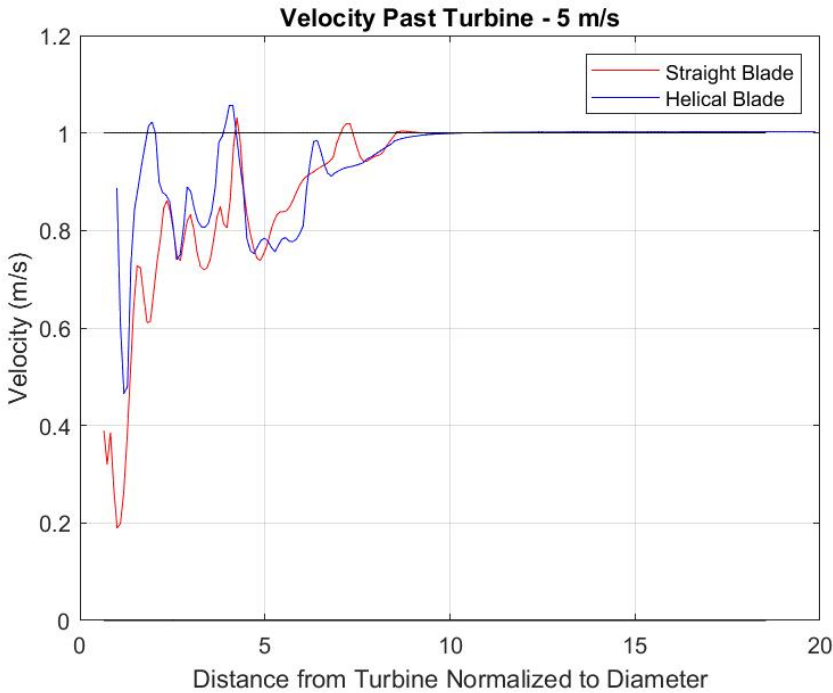
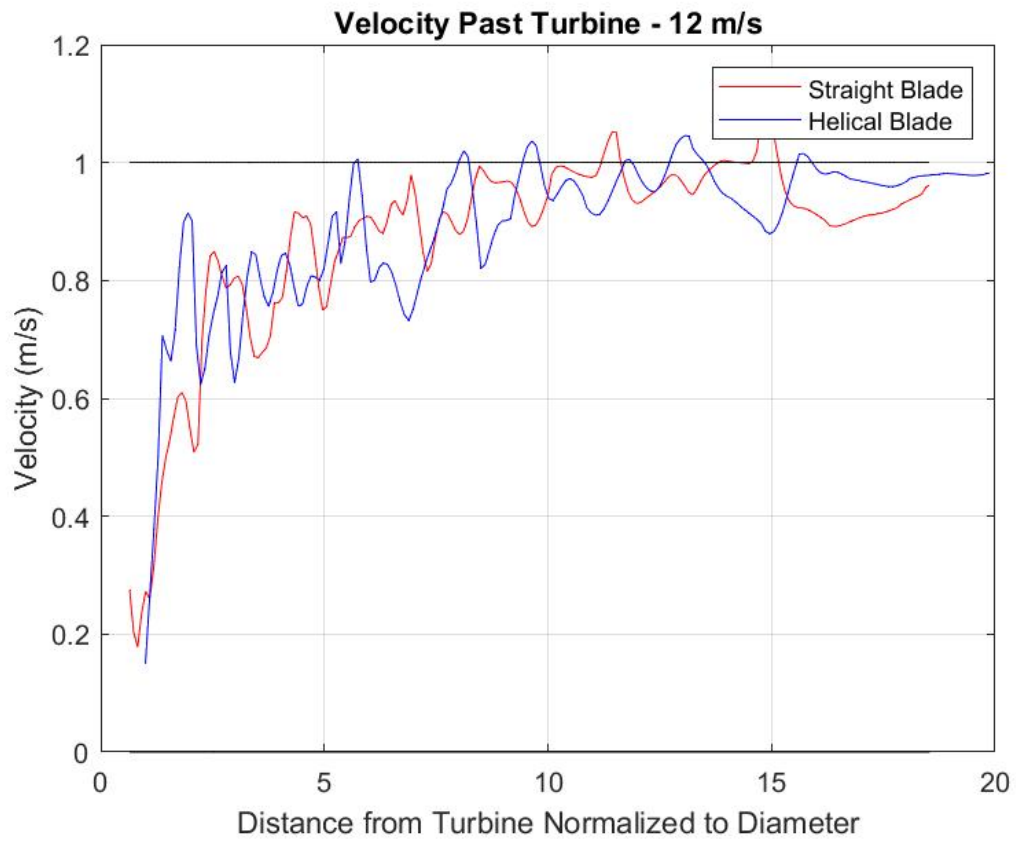(2): Velocity Recovery Plot for helical and straight blade designs at 7 m/s.
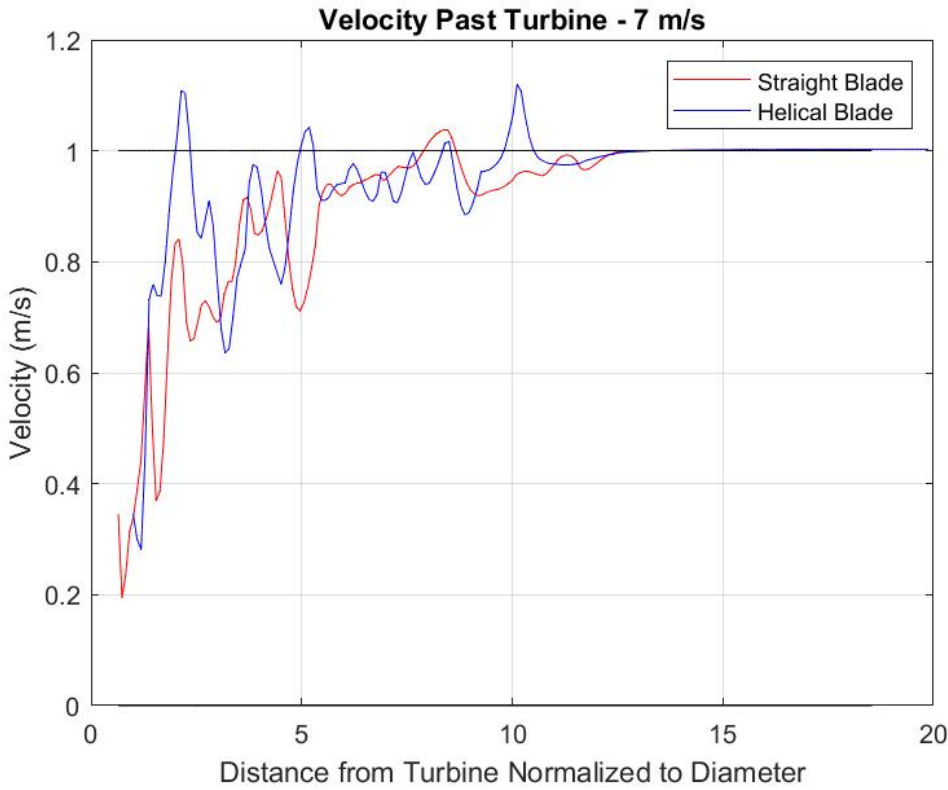
(3): Velocity Recovery Plot for helical and straight blade designs at 9 m/s.

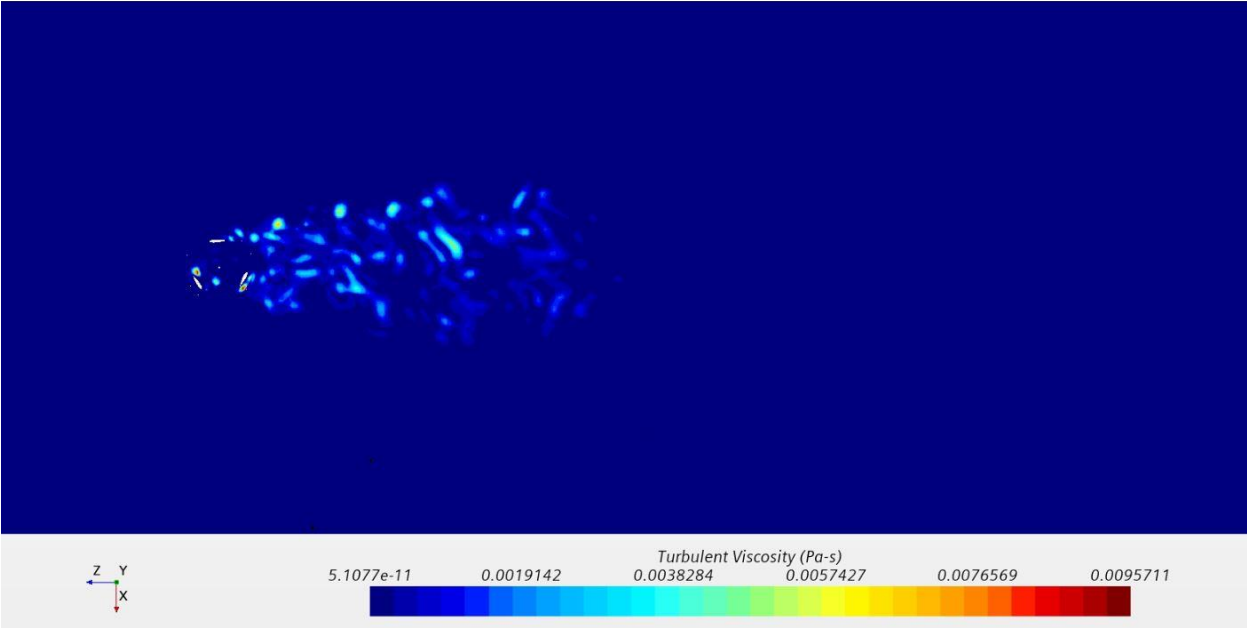(4): Velocity Recovery Plot for helical and straight blade designs at 10 m/s.

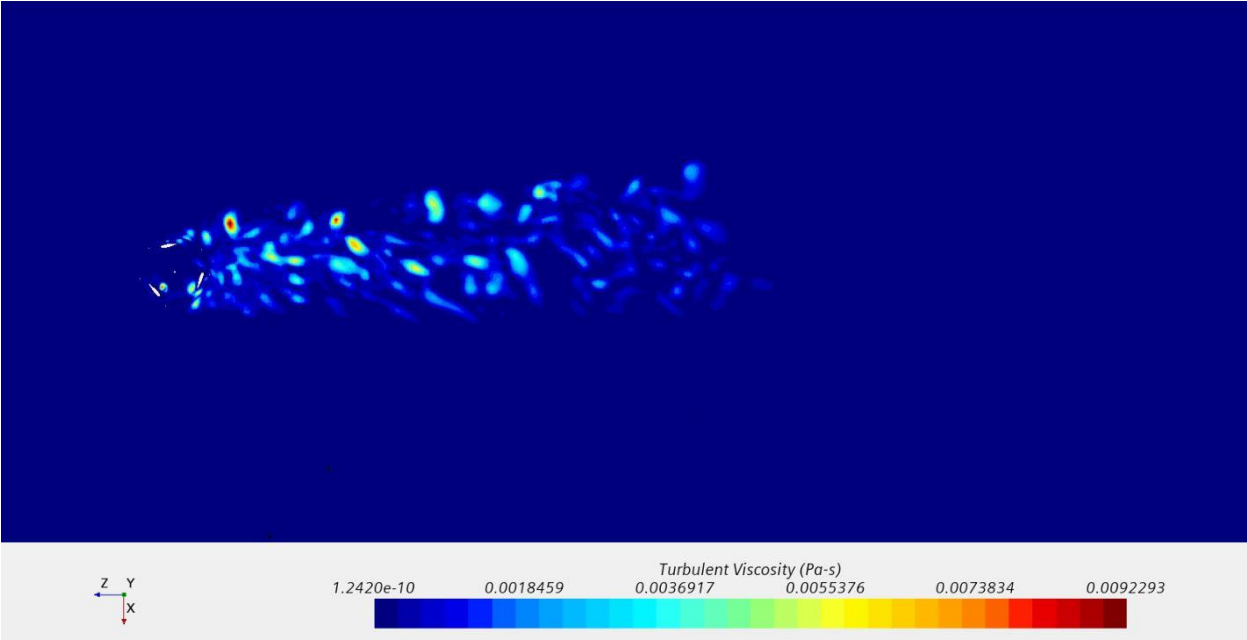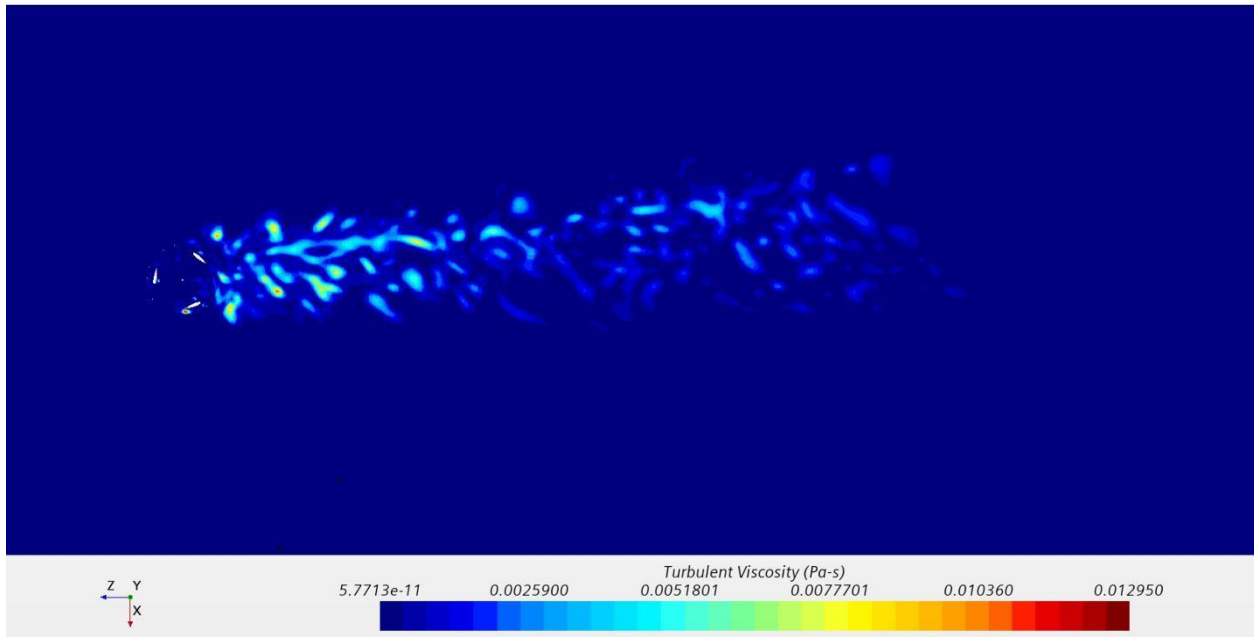(5): Velocity Recovery Plot for helical and straight blade designs at 12 m/s.

11 Appendix B:

(1) Turbulent viscosity field for helical turbine at 5 m/s wind velocity.

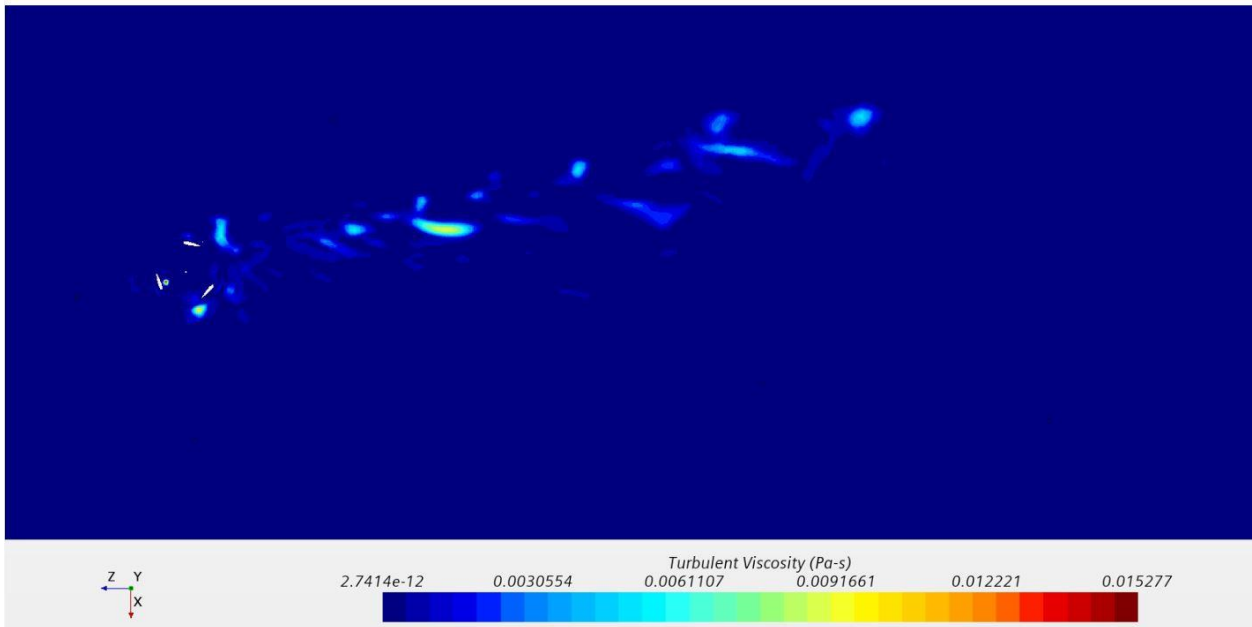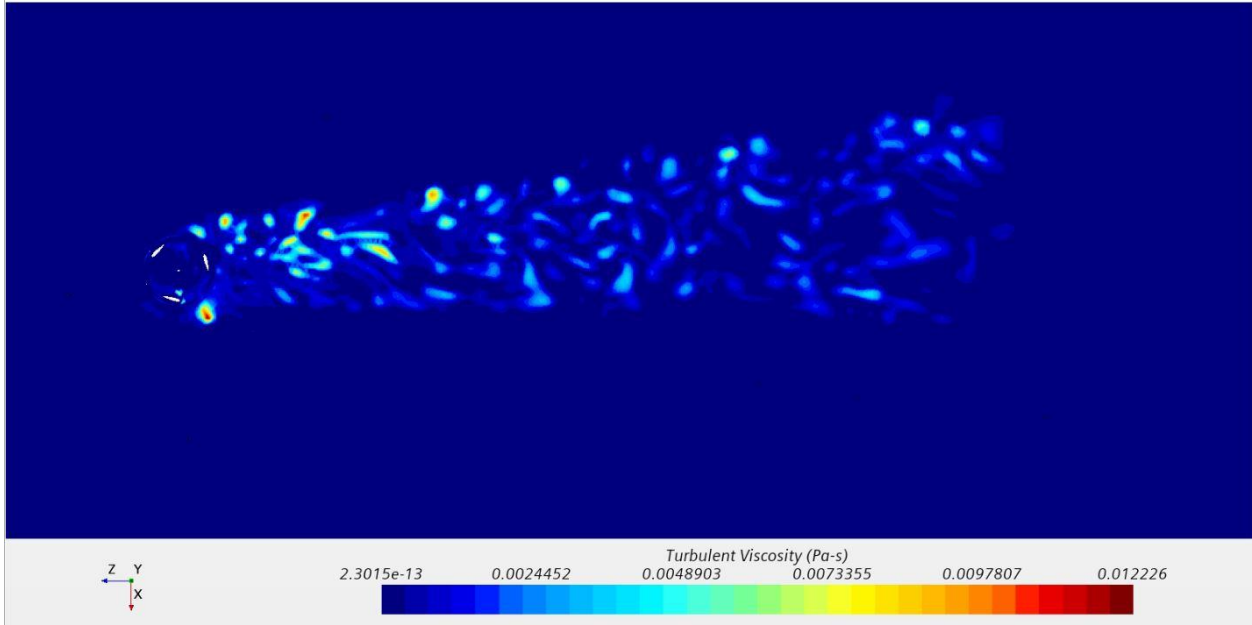(2) Turbulent viscosity field for helical turbine at 7 m/s wind velocity.

(3) Turbulent viscosity field for helical turbine at 9 m/s wind velocity.

(4) Turbulent viscosity field for helical turbine at 10 m/s wind velocity.
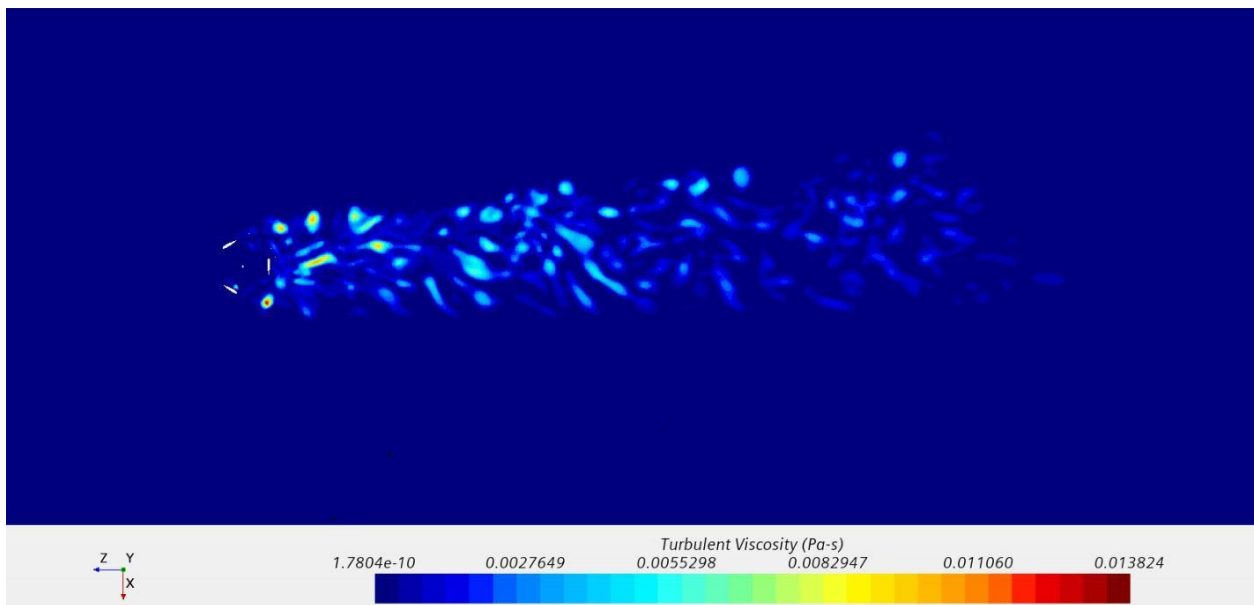
(5) Turbulent viscosity field for helical turbine at 12 m/s wind velocity.
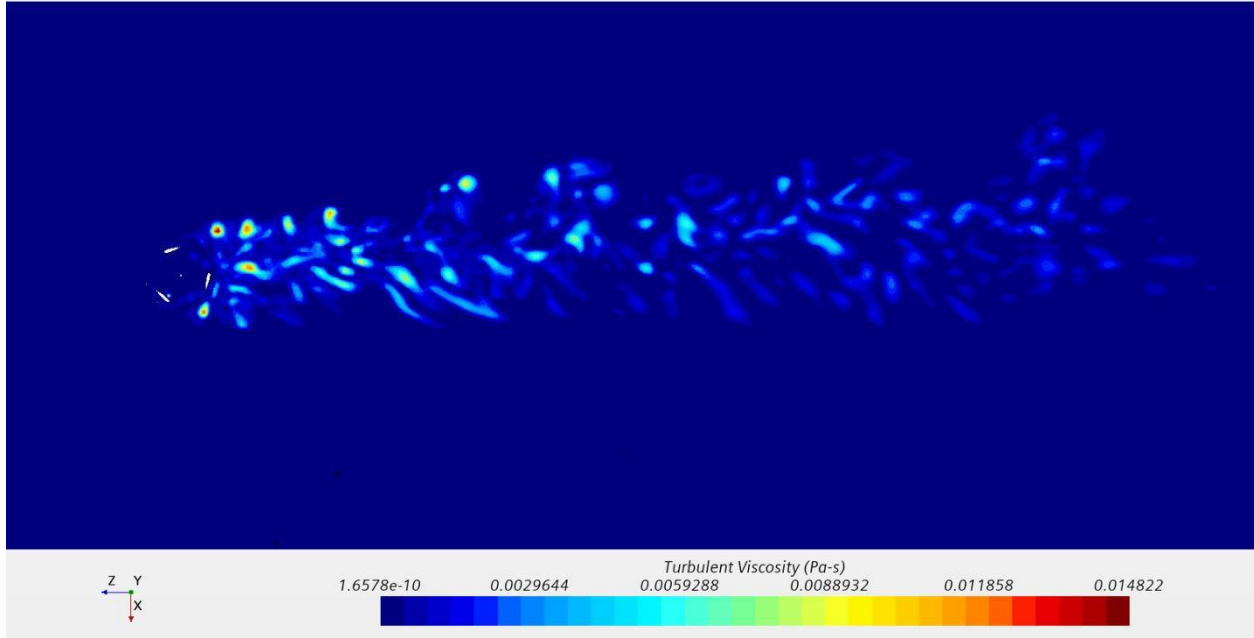
(6) Turbulent viscosity field for straight turbine at 5 m/s wind velocity.
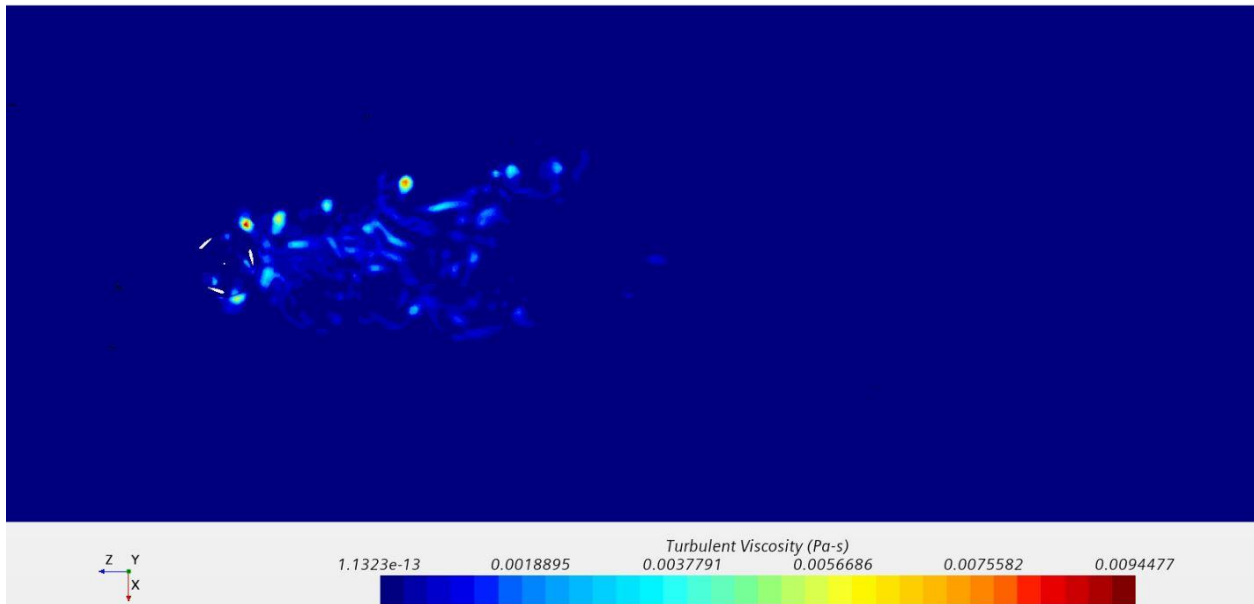
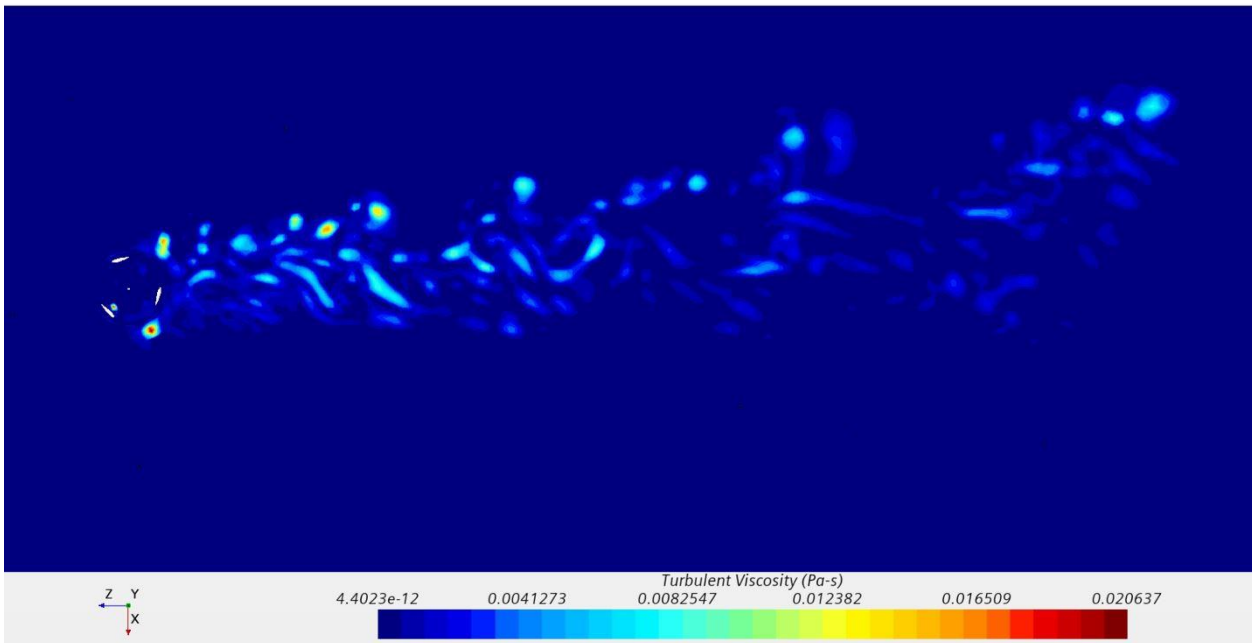(7) Turbulent viscosity field for straight turbine at 7 m/s wind velocity.

Turbulent Viscosity (Pa-s)

| 1.4766e-11 | 0.0019909 | 0.0039818 | 0.0059728 | 0.0079637 | 0.0099546 |
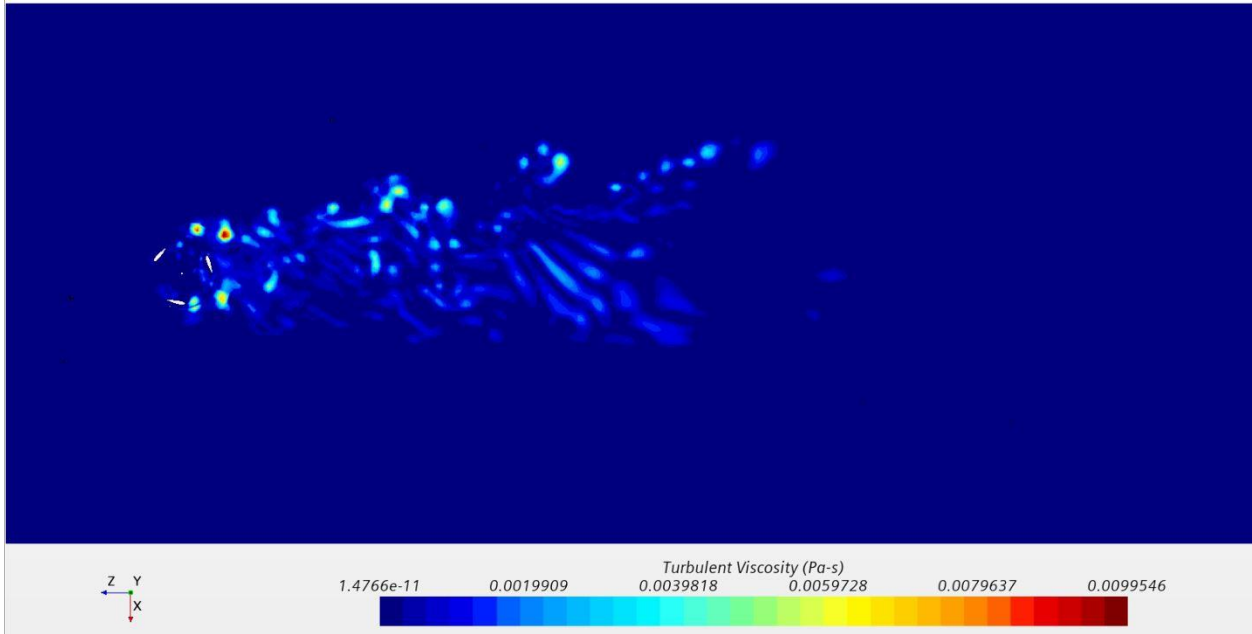
(8) Turbulent viscosity field for straight turbine at 9 m/s wind velocity.

Turbulent Viscosity (Pa-s)

| 2.7414e-12 | 0.0030554 | 0.0061107 | 0.0091661 | 0.012221 | 0.015277 |

(9) Turbulent viscosity field for straight turbine at 10 m/s wind velocity.

Turbulent Viscosity (Pa-s)

| 2.3015e-13 | 0.0024452 | 0.0048903 | 0.0073355 | 0.0097807 | 0.012226 |

(10)Turbulent viscosity field for straight turbine at 12 m/s wind velocity.

Turbulent Viscosity (Pa-s)

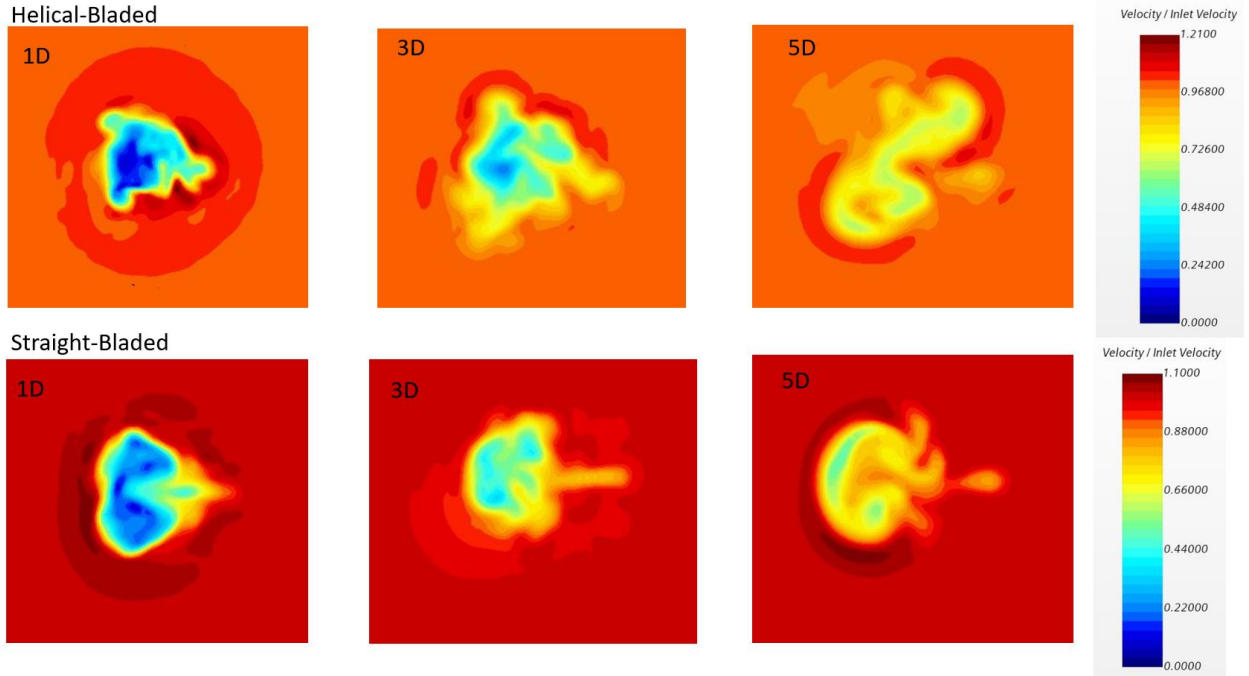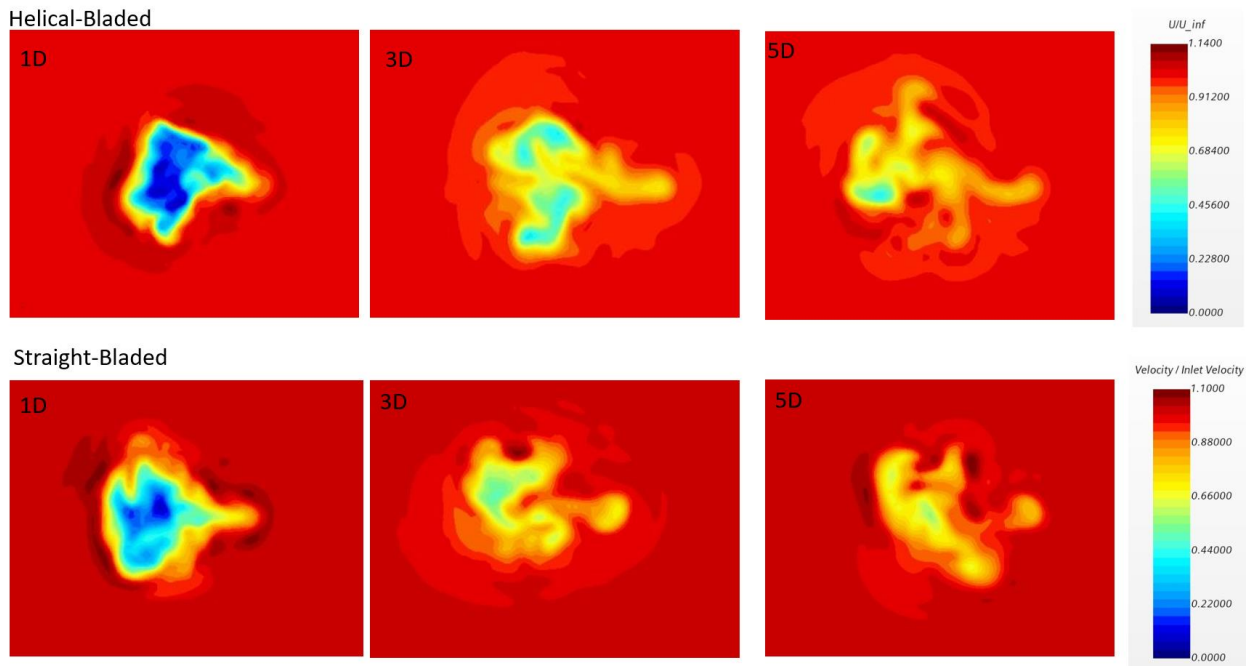| 4.4023e-12 | 0.0041273 | 0.0082547 | 0.012382 | 0.016509 | 0.020637 |

12 Appendix C:

(1) Velocity Recovery Plane Sections – Helical vs Straight Bladed – 5 m/s
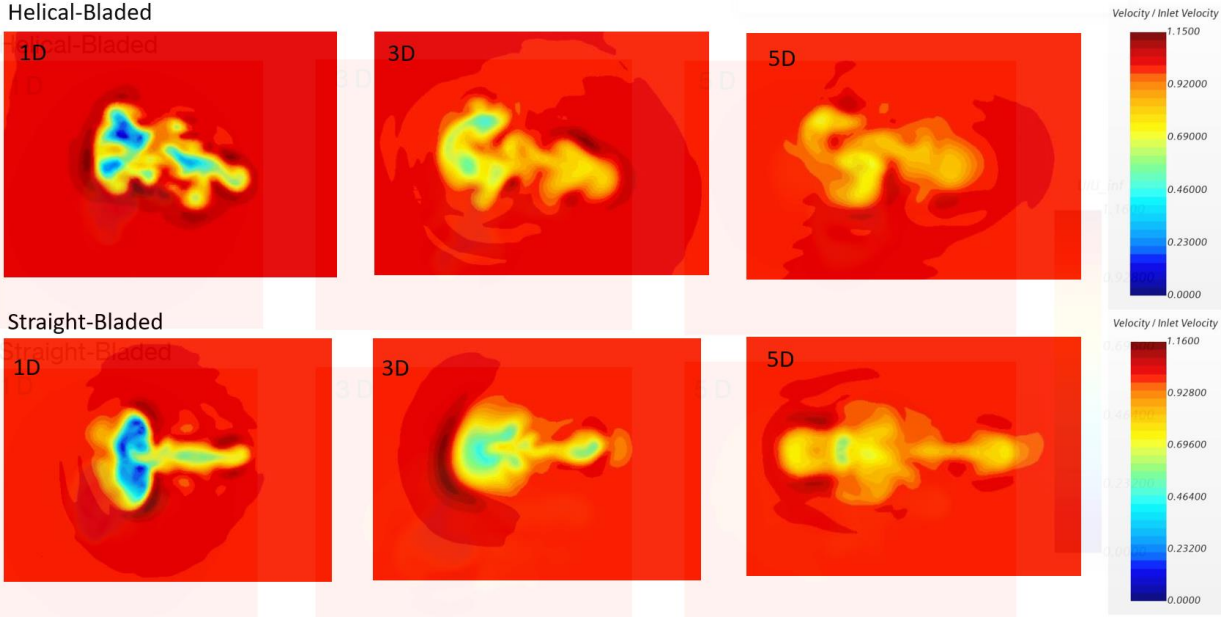
(2) Velocity Recovery Plane Sections – Helical vs Straight Bladed – 7 m/s
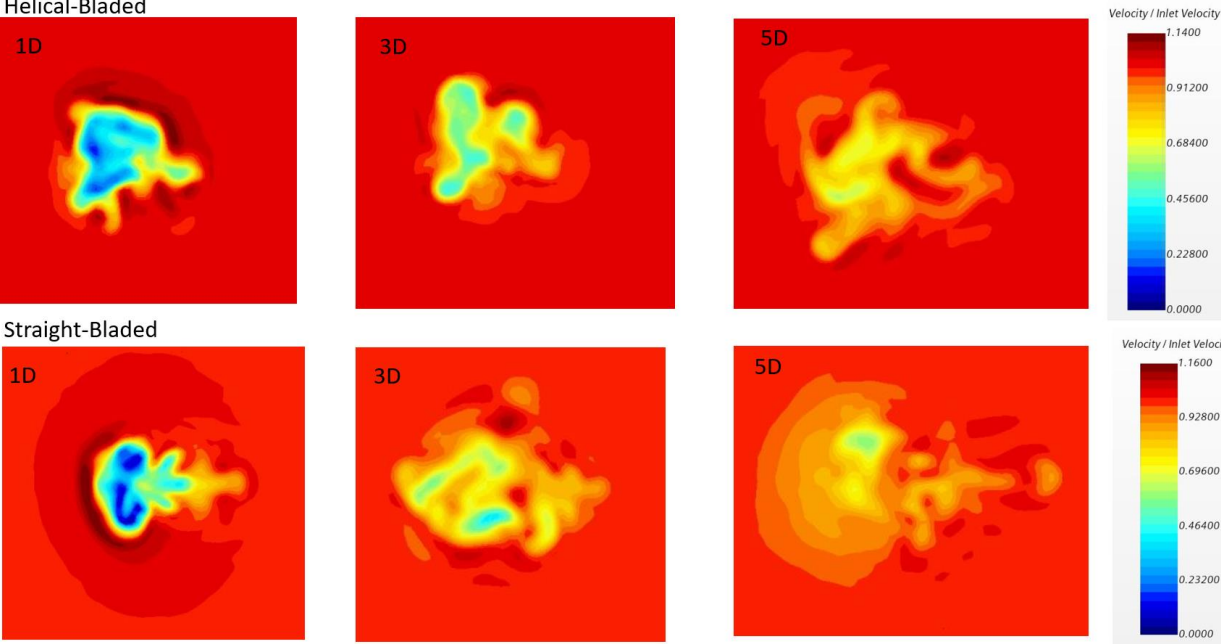
(3) Velocity Recovery Plane Sections – Helical vs Straight Bladed – 9 m/s
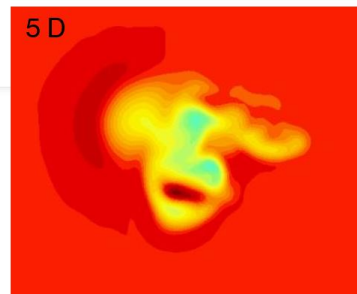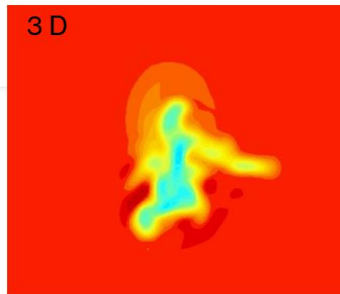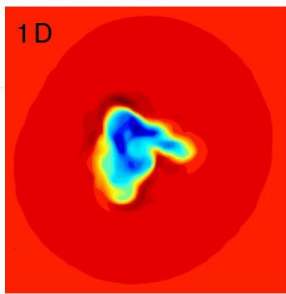
(4) Velocity Recovery Plane Sections – Helical vs Straight Bladed – 10 m/s

(5) Velocity Recovery Plane Sections – Helical vs Straight Bladed – 12 m/s

Helical-Bladed

1 D   3 D   5 D

Straight-Bladed

1 D   3 D   5 D

U/U_inf

1.1600

0.92800

0.69600

0.46400

0.23200

0.0000